Numerical meshes ensuring uniform observability of $1d$ waves: construction and analysis*

Sylvain Ervedoza† Aurora Marica‡ Enrique Zuazua§

April 23, 2015

Abstract

We build non-uniform numerical meshes for the finite difference and finite element approximations of the $1d$ wave equation, ensuring that all numerical solutions reach the boundary, as continuous solutions do, in the sense that the full discrete energy can be observed by means of boundary measurements, uniformly with respect to the mesh-size. The construction of the non-uniform mesh is achieved by means of a concave diffeomorphic transformation of a uniform grid into a non-uniform one, making the mesh finer and finer when approaching the right boundary. For uniform meshes it is known that high-frequency numerical wave packets propagate very slowly without never getting to the boundary. Our results show that this pathology can be avoided by taking suitable non-uniform meshes. This also allows to build convergent numerical algorithms for the approximation of boundary controls of the wave equation.

1 Introduction

The goal of this article is to build non-uniform numerical meshes for the numerical approximation of the $1d$ wave equation, ensuring that all numerical solutions reach the boundary, as continuous solutions do. This is relevant for boundary control problems, but also in the context of inverse problems where detection from the boundary requires that waves get there.

For simplicity, we will focus on the constant coefficient $1d$ wave equation

$$\begin{cases} \partial_{tt}u - \partial_{xx}u = 0, & (t,x) \in (0,T)\times(0,1), \\ u(t,0) = u(t,1) = 0, & t \in (0,T), \\ u(0,x) = u^0(x),\ \partial_t u(0,x) = u^1(x), & x \in (0,1). \end{cases} \tag{1.1}$$

*The research of the third author was funded by the Advanced Grant FP7-246775 NUMERIWAVES of the European Research Council Executive Agency, FA9550-14-1-0214 of the EOARD-AFOSR, FA9550-15-1-0027 of AFOSR, the BERC 2014-2017 program of the Basque Government, the MTM2011-29306-C02-00 and SEV-2013-0323 Grants of the MINECO and a Humboldt Award at the University of Erlangen-Nürnberg. Part of this work was done during the postdoc stay of the second author at Institute of Mathematics and Scientific Computing and University of Graz, funded by the MOBIS - Mathematical Optimization and Applications in Biomedical Sciences grant of the FWF - Austrian Science Fund. The second author's work was also supported by two grants of the Romanian Ministry of National Education (CNCS-UEFISCDI), projects PN-II-ID-PCE-2012-4-0021 *Variable Exponent Analysis: PDEs and Calculus of Variations* and PN-II-ID-PCE-2011-3-0075 *Analysis, control and numerical approximations of PDEs.* The second and third authors thank the CIMI Excellence Laboratory, Toulouse, France, for hospitality and support during the preparation of this work in the context of the Excellence Chair in *PDEs, Control and Numerics.*

†Institut de Mathématiques de Toulouse; UMR5219; Université de Toulouse; CNRS; UPS IMT, F-31062, Toulouse Cedex 9, France, sylvain.ervedoza@math.univ-toulouse.fr.

‡Faculty of Applied Sciences, University Politehnica of Bucharest, Romania, auroramarica@yahoo.com.

§BCAM - Basque Center for Applied Mathematics, Alameda Mazarredo 14, 48009, Bilbao, Basque Country, Spain, and Ikerbasque - Basque Foundation for Science, Maria Diaz de Haro 3, 48013, Bilbao, Basque Country, Spain, zuazua@bcamath.org.

To fix our ideas and better establish the requirements that we impose on the numerical mesh we address the problem from the perspective of the so-called *observability inequality* according to which the solutions of (1.1) satisfy

$$\left\|(u^0,u^1)\right\|_{H_0^1(0,1)\times L^2(0,1)} \leq C_{obs}\left\|\partial_x u(t,1)\right\|_{L^2(0,T)}, \tag{1.2}$$

for a suitable constant $C_{obs}=C_{obs}(T)>0$ provided $T\geq 2$.

Note that inequality (1.2) ensures that all waves propagating in space-time according to the wave equation reach the extreme $x=1$ in time $T=2$. This is in agreement with the well-known properties of solutions of the wave equation that can be proved easily based on the Fourier or d'Alembert representation formulas.

This inequality, by duality, ensures the exact controllability of the wave equation when the control acts on the boundary $x=1$, see e.g. [18].

In the pioneering works [13, 14] on the numerical approximation of boundary controls for the wave equation, it was shown that naive discretizations of the wave equation (1.1) may lead to the divergence of numerical controls. This is due to the fact that discrete approximations of the wave equation (1.1) are, in general, not uniformly observable. In other words, in general, discrete versions of the observability inequality (1.2) do not hold uniformly with respect to the mesh-size parameter.

This phenomenon has been analysed and explained starting with the work [16] dealing with finite differences and finite element methods on uniform meshes, and later on generalized in several directions. We refer to the survey articles [10, 28] for an account of the most recent developments. But, until now, most often, the analysis was restricted to uniform meshes. More general meshes were considered in [23] viewing numerical solutions as quasi-solutions of the continuous wave model. Accordingly, severe filtering mechanisms on the numerical high-frequency components were required to conclude uniform observability inequalities.

More recently, in [20], the problem of the propagation of high-frequency numerical solutions was considered in non-uniform meshes built through a diffeomorphic deformation of a uniform one. Using microlocal tools, the notions of numerical symbol and bicharacteristic rays were introduced and it was shown both analytically and through numerical simulations, that high-frequency numerical wave packets follow, in space-time, the path indicated by the bicharacteristics.

The present work complements previous ones, addressing the problem from a different perspective. In here our aim is to design meshes so to ensure that all numerical waves reach the boundary. This makes, accordingly, the discrete version of (1.2) to hold uniformly with respect to the mesh-size parameter. In other words, the meshes we build are well-adapted to the boundary observability property under consideration.

To our knowledge, this result is the first one in this direction and opens up new interesting perspectives of development, for instance, to multi-dimensional problems or with inverse problem applications in view.

To begin with, we introduce the space semi-discrete approximations of (1.1) on a non-uniform mesh obtained by a diffeomorphic deformation of a uniform one.

Let $g:[0,1]\to[0,1]$ denote a diffeomorphism of the interval $[0,1]$. For $N\in\mathbb{N}$, we set $h:=1/(N+1)$ and consider the non-uniform mesh given by the nodes

$$x_j:=g(jh),\quad \forall j\in\{0,\cdots,N+1\}, \tag{1.3}$$

yielding the heterogeneous mesh-sizes

$$h_{j+1/2}:=x_{j+1}-x_j,\quad \forall j\in\{0,\cdots,N\},\qquad \text{and}\qquad h_j:=\frac{h_{j-1/2}+h_{j+1/2}}{2},\quad \forall j\in\{1,\cdots,N\}. \tag{1.4}$$

In the following, we will use the notation $\mathscr{M}^{h,g}$ to refer to the mesh given by (1.3)–(1.4), i.e., $\mathscr{M}^{h,g}:=\{x_j,\, j\in\{0,\cdots,N+1\}\}$.

The space semi-discretization of the wave equation (1.1) obtained by finite differences on this non-uniform mesh $\mathscr{M}^{h,g}$ reads as follows:

$$\begin{cases} h_j u_j''(t) - \Big(\dfrac{u_{j+1}(t)-u_j(t)}{h_{j+1/2}} - \dfrac{u_j(t)-u_{j-1}(t)}{h_{j-1/2}}\Big) = 0, & t\in(0,T),\ 1\le j\le N,\\ u_0(t) = u_{N+1}(t) = 0, & t\in(0,T),\\ u_j(0) = u_j^0,\ u_j'(0) = u_j^1, & 1\le j\le N. \end{cases} \tag{1.5}$$

To avoid possible confusions, when needed, we will denote the solutions of (1.5) by $\mathbf{u}^{h,g}(t) = (u_j^g(t))_{0\le j\le N+1}$, where g stands for the diffeomorphic transformation from the uniform to the non-uniform mesh and $h := 1/(N+1)$ is the mesh-size. But, in general, we will simply write down $\mathbf{u}^h(t) = (u_j(t))_{0\le j\le N+1}$ for the solutions of (1.5).

System (1.5) enjoys the property of energy conservation. In other words, the energy

$$E^{h,g}(\mathbf{u}^{h,g}(t), \partial_t \mathbf{u}^{h,g}(t)) := \frac{1}{2}\sum_{j=1}^{N} h_j |u_j'(t)|^2 + \frac{1}{2}\sum_{j=0}^{N} h_{j+1/2}\Big|\frac{u_{j+1}(t)-u_j(t)}{h_{j+1/2}}\Big|^2 \tag{1.6}$$

is constant in time and coincides with the initial energy $E^{h,g}(\mathbf{u}^{0,h}, \mathbf{u}^{1,h})$. This ensures the stability of the numerical scheme and also its convergence in the classical sense of numerical analysis.

The main result of this paper is the following:

Theorem 1.1. *Given $T > 2$, there exists a smooth diffeomorphism g such that the solutions $\mathbf{u}^{h,g}$ of (1.5) are uniformly observable through $x = 1$ in time T. To be more precise, there exist $h^\star = h^*(T,g) > 0$ and a constant $C_{obs}^g = C_{obs}^g(T) > 0$ (independent of h) such that, for all $h \in (0, h^\star)$, the solutions $\mathbf{u}^{h,g}$ on the mesh $\mathscr{M}^{h,g}$ satisfy the observability inequality:*

$$E^{h,g}(\mathbf{u}^{0,h}, \mathbf{u}^{1,h}) \le (C_{obs}^g)^2 \int_0^T \left|\frac{u_N^g(t)}{h_{N+1/2}}\right|^2 dt. \tag{1.7}$$

More precisely, g can be chosen explicitly as

$$g_\theta(x) = \sqrt{(2\theta+1)x+\theta^2} - \theta, \qquad \text{for } \theta \in \left(0, \frac{T-2}{2}\right). \tag{1.8}$$

Theorem 1.1 may appear surprising in view of the negative results in [16], and later on refined in [22], showing the divergence of the observability constant $C_{obs}^g(T)$ in (1.7) (of the order of $\exp(c/h)$) for the uniform mesh. On uniform meshes the cause of this divergence is the existence of high-frequency numerical solutions that remain trapped within the computational domain without never getting to its boundary. Theorem 1.1 shows that one can design a suitable mesh for a given observability problem, so to assure that all numerical waves are guided towards the subset where the observation is being done. In this sense, Theorem 1.1 is close to the works [5, 6], where a suitable (optimal) mesh was designed in order to provide accurate results on the inverse Sturm-Liouville problem. In particular, in these references it was shown that, when trying to recover the conductivity coefficient σ out of some a priori guess σ_0 of the unknown coefficient, using measurements of the Neumann-to-Dirichlet map at $x = 0$, optimal grids need to be finer close to the point $x = 0$ where measurements are performed.

Actually, Theorem 1.1 is deduced from the following more general result:

Theorem 1.2. *Let $g : [0,1] \to [0,1]$ be a $C^3([0,1])$ diffeomorphism satisfying $g(0) = 0$, $g(1) = 1$, and assume that g is strictly concave. Define θ_g by*

$$\theta_g := \max_{x\in[0,1]} \left\{ \frac{g'(x)^2 + g(x)g''(x)}{-g''(x)} \right\}. \tag{1.9}$$

Then the solutions $\mathbf{u}^{h,g}$ *of* (1.5) *are uniformly observable through* $x = 1$ *in any time* $T > T_g$*, where* T_g *is the multiplier time given by*

$$T_g := 2(1 + \theta_g). \tag{1.10}$$

Note that the strict concavity condition in Theorem 1.2 implies that g' is strictly decreasing on the whole space interval $[0, 1]$. The corresponding mesh given by (1.3) therefore decreases gradually from the coarsest scale $h_{1/2}$ to the finest one $h_{N+1/2}$ located at the endpoint $x = 1$ where the observation is performed. This corresponds to the very natural fact that much more precise information is required close to the observation set, which needs a refined mesh.

In any case, it is important to observe that the meshes under consideration involve only one single scale. Indeed, if g satisfies the assumptions of Theorem 1.2, the mesh given by (1.3) is quasi-uniform, the ratio $h_{1/2}/h_{N+1/2}$ between the largest and the smallest mesh sizes being uniformly bounded from above:

$$1 \leq \frac{h_{1/2}}{h_{N+1/2}} \leq C := \frac{\max g'}{\min g'} = \frac{g'(0)}{g'(1)}.$$

Note that, according to the assumption that g is a diffeomorphism of $[0, 1]$, the derivative g' cannot vanish or blow up at any point $x \in [0, 1]$ and then the above constant C is finite.

Outline of the paper. In Section 2, we provide the detailed proof of Theorems 1.1–1.2. We will first present the proof of Theorem 1.2. It will be based on a suitable multiplier argument performed on the discrete solutions $\mathbf{u}^{h,g}$ of (1.5), mimicking the continuous multiplier technique (cf. [18]). While it is well-known that the multiplier technique does not yield uniform observability results in the context of uniform meshes [16], our computations will put in evidence a new reminder term involving the second-order derivative of g. Once this is done, the proof of Theorem 1.2 consists in a suitable analysis of that new term.

In Section 3, we then provide two insights on the results in Theorems 1.1 and 1.2, addressing them from the spectral point of view and also from the microlocal perspective.

• The first interpretation will be based on the analysis of the spectrum of the discrete spatial operator in (1.5). While the spectrum of the discrete Laplacian on a uniform mesh is equidistributed on the domain $(0, 1)$, being given by the restriction of the continuous eigenfunctions $x \mapsto \sqrt{2}\sin(k\pi x)$ to the discrete mesh, they are not uniformly distributed anymore when the domain $(0, 1)$ is discretized using the mesh (1.3) obtained by applying a strictly concave diffeomorphism g to a uniform mesh. To be more precise, as we shall see for the specific examples of $g = g_\theta$ as in (1.8) for various choices of θ, the eigenvectors corresponding to the high-frequency eigenvalues concentrate on the refined part of the mesh, namely close to $x = 1$ (see Figures 2–3). Actually, this phenomenon was already observed in the work [7] corresponding to the case of a space discretization based on mixed finite elements. One can furthermore check experimentally that the dispersion diagram presents a significant gap when the domain $(0, 1)$ is discretized using the mesh (1.3) corresponding to g_θ in (1.8), while the gap vanishes when the mesh is uniform. Ingham's lemma [17] could then possibly be used to prove Theorem 1.1. But this would require a careful description of the spectrum of the discrete Laplace operator on non-uniform meshes of the form (1.3), that is to be done.

• The second one consists in analysing the behavior of the rays of Geometric Optics on meshes obtained by applying a diffeomorphism g to a uniform mesh. It is well-known that, for the continuous wave equation (1.1) all rays propagate at velocity one, but that the space semi-discrete wave equations (1.5) may generate many more dynamics, with different propagation properties at high-frequencies. For instance, on a uniform mesh, one can generate spurious high-frequency solutions traveling at arbitrarily small velocities [26]. On a non-uniform mesh, the situation is even more intricate. As indicated in [27] and [20], for some numerical grids, the rays of Geometric Optics may present internal reflections generated by the mesh.

The analysis in [20] shows that the rays corresponding to frequencies of the order of $1/h$ obey the

following Hamiltonian flow:

$$H(t,x,\tau,\xi) = -g'(x)\tau^2 + \frac{4}{g'(x)}\sin^2\left(\frac{\xi}{2}\right). \tag{1.11}$$

We will check experimentally that, on the non-uniform meshes given by g_θ in (1.8), these rays are curved by the mesh in such a way that they all hit the boundary $x = 1$ in times less than T_g.

We will provide a formula for the computation of the characteristic time $T_{g,char}$ on non-uniform meshes given by any strictly concave diffeomorphisms g via microlocal analysis and we will compare it numerically with the multiplier time T_g in (1.10) for $g = g_\theta$ in (1.8).

In Section 4, as a consequence of the uniform observability inequality, we perform some numerical experiments showing that the corresponding controllability problem for (1.1) can be solved without any filtering, in contrast with the behaviour of classical numerical schemes on uniform meshes.

In Section 5, we extend Theorems 1.1 and 1.2 to the P_1 finite element space semi-discretization on non-uniform meshes given by strictly concave diffeomorphisms g. In particular, we show that the P_1 finite element approximation of (1.1) enjoys uniform observability properties in time T_g as in (1.10), see Theorem 5.1. Our study follows the discrete multiplier approach of the finite difference case, though more technically involved.

In Section 6, we discuss some other closely related issues and indicate some possible directions of future research.

2 Proof of Theorems 1.1–1.2

As indicated in the introduction, the proof of Theorem 1.2 is based on a multiplier technique mimicking the proof in [18] for the continuous wave equation (1.1), which basically consists in multiplying equation (1.1) by $x\partial_x u$ and performing integrations by parts in both space and time variables.

Accordingly, we will multiply the equation (1.5) by a discrete version of the multiplier $x\partial_x u$, namely

$$m_j(t) := \frac{\theta_j}{2}\left(\frac{u_{j+1}(t)-u_j(t)}{h_{j+1/2}} + \frac{u_j(t)-u_{j-1}(t)}{h_{j-1/2}}\right), \quad t\in(0,T),\ j\in\{1,\cdots,N\}, \tag{2.1}$$

where $\mathbf{u}^h(t) = (u_j(t))_{0\le j\le N+1}$ solves (1.5) and the coefficients θ_j will be chosen later on.

2.1 A discrete multiplier identity

We start with the following result:

Proposition 2.1 (A discrete multiplier identity)**.** *If $\mathbf{u}^h(t)$ solves the equation* (1.5) *and $\mathbf{m}^h(t)$ denotes the multiplier in* (2.1)*, the following identity holds:*

$$\begin{aligned}\sum_{j=1}^N h_j u_j'(t) m_j(t)\Big|_0^T &+ \frac14\sum_{j=1}^N\int_0^T\left(\frac{\theta_{j+1}h_{j+1}+\theta_j h_j}{h_{j+1/2}} - \frac{\theta_j h_j+\theta_{j-1}h_{j-1}}{h_{j-1/2}}\right)|u_j'(t)|^2\,dt\\ &- \frac14\sum_{j=0}^N\int_0^T h_{j+1/2}(\theta_{j+1}h_{j+1}-\theta_j h_j)\left|\frac{u_{j+1}'(t)-u_j'(t)}{h_{j+1/2}}\right|^2 dt\\ &+\frac12\sum_{j=0}^N\int_0^T(\theta_{j+1}\ -\theta_j)\left|\frac{u_{j+1}(t)-u_j(t)}{h_{j+1/2}}\right|^2 dt + \frac{\theta_0}{2}\int_0^T\left|\frac{u_1(t)}{h_{1/2}}\right|^2 dt = \frac{\theta_{N+1}}{2}\int_0^T\left|\frac{u_N(t)}{h_{N+1/2}}\right|^2 dt,\end{aligned} \tag{2.2}$$

where h_0 and h_{N+1} can be set arbitrarily.

Proof. Multiplying the equation (1.5) by m_j in (2.1), summing on $j \in \{1, \cdots, N\}$ and integrating in time, we obtain

$$A - B = 0, \text{ with } A = \sum_{j=1}^{N} \int_0^T h_j u_j''(t) m_j(t)\, dt$$

$$\text{and } B = \sum_{j=1}^{N} \int_0^T \left(\frac{u_{j+1}(t) - u_j(t)}{h_{j+1/2}} - \frac{u_j(t) - u_{j-1}(t)}{h_{j-1/2}} \right) m_j(t)\, dt.$$

We now compute separately A and B.

Computation of A. By integration by parts in time, we get

$$A = \sum_{j=1}^{N} h_j u_j'(t) m_j(t) \Big|_0^T - A^0, \quad \text{with } A^0 = \sum_{j=1}^{N} \int_0^T h_j u_j'(t) m_j'(t)\, dt.$$

and easy computations yield

$$\begin{aligned} A^0 &= \frac{1}{2} \sum_{j=1}^{N} \int_0^T \theta_j h_j u_j'(t) \left(\frac{u_{j+1}'(t) - u_j'(t)}{h_{j+1/2}} \right) dt + \frac{1}{2} \sum_{j=1}^{N} \int_0^T \theta_j h_j u_j'(t) \left(\frac{u_j'(t) - u_{j-1}'(t)}{h_{j-1/2}} \right) dt \\ &= \frac{1}{2} \sum_{j=0}^{N} \int_0^T \theta_j h_j u_j'(t) \left(\frac{u_{j+1}'(t) - u_j'(t)}{h_{j+1/2}} \right) dt + \frac{1}{2} \sum_{j=0}^{N} \int_0^T \theta_{j+1} h_{j+1} u_{j+1}'(t) \left(\frac{u_{j+1}'(t) - u_j'(t)}{h_{j+1/2}} \right) dt \\ &= \frac{1}{2} \sum_{j=0}^{N} \int_0^T (\theta_j h_j u_j'(t) + \theta_{j+1} h_{j+1} u_{j+1}'(t)) \left(\frac{u_{j+1}'(t) - u_j'(t)}{h_{j+1/2}} \right) dt. \end{aligned}$$

In the above computations, h_0 and h_{N+1} can be chosen arbitrarily as they are multiplied by $u_0'(t) = 0$ and $u_{N+1}'(t) = 0$ and do not really appear in the computations. Writing

$$\theta_j h_j u_j' + \theta_{j+1} h_{j+1} u_{j+1}' = \frac{1}{2}(\theta_{j+1} h_{j+1} + \theta_j h_j)(u_{j+1}' + u_j') + \frac{1}{2}(\theta_{j+1} h_{j+1} - \theta_j h_j)(u_{j+1}' - u_j'),$$

we get

$$A^0 = A^1 + \frac{1}{4} \sum_{j=0}^{N} \int_0^T h_{j+1/2} (\theta_{j+1} h_{j+1} - \theta_j h_j) \left| \frac{u_{j+1}'(t) - u_j'(t)}{h_{j+1/2}} \right|^2 dt,$$

$$\text{with } A^1 = \frac{1}{4} \sum_{j=0}^{N} \int_0^T (\theta_{j+1} h_{j+1} + \theta_j h_j) \left(\frac{|u_{j+1}'(t)|^2 - |u_j'(t)|^2}{h_{j+1/2}} \right) dt,$$

and A^1 can be simplified as:

$$A^1 = -\frac{1}{4} \sum_{j=1}^{N} \int_0^T \left(\frac{\theta_{j+1} h_{j+1} + \theta_j h_j}{h_{j+1/2}} - \frac{\theta_j h_j + \theta_{j-1} h_{j-1}}{h_{j-1/2}} \right) |u_j'(t)|^2\, dt.$$

The *computation of* B is straightforward:

$$\begin{aligned}
B &= \sum_{j=1}^{N} \int_0^T \left(\frac{u_{j+1}(t)-u_j(t)}{h_{j+1/2}} - \frac{u_j(t)-u_{j-1}(t)}{h_{j-1/2}} \right) \frac{\theta_j}{2} \left(\frac{u_{j+1}(t)-u_j(t)}{h_{j+1/2}} + \frac{u_j(t)-u_{j-1}(t)}{h_{j-1/2}} \right) dt \\
&= \frac{1}{2} \sum_{j=1}^{N} \int_0^T \theta_j \left(\left| \frac{u_{j+1}(t)-u_j(t)}{h_{j+1/2}} \right|^2 - \left| \frac{u_j(t)-u_{j-1}(t)}{h_{j-1/2}} \right|^2 \right) dt \\
&= -\sum_{j=0}^{N} \int_0^T \frac{\theta_{j+1}-\theta_j}{2} \left| \frac{u_{j+1}(t)-u_j(t)}{h_{j+1/2}} \right|^2 dt + \frac{\theta_{N+1}}{2} \int_0^T \left| \frac{u_N(t)}{h_{N+1/2}} \right|^2 dt - \frac{\theta_0}{2} \int_0^T \left| \frac{u_1(t)}{h_{1/2}} \right|^2 dt. \quad (2.3)
\end{aligned}$$

Putting together the above computations we immediately get the identity (2.2). □

2.2 Choice of the multiplier θ_j

For the sake of clarity, it is convenient to employ the Landau notation $\mathcal{O}$. In the following, for g a diffeomorphism of $[0,1]$ satisfying $g(0)=0$ and $g(1)=1$, $\mathcal{O}(h^\alpha)$ will denote a function $f(h,x)$ such that there exist $h^*>0$ and $C>0$ such that for all $h\in(0,h^*)$ and $x_j \in \mathscr{M}^{h,g}$,

$$|f(h,x_j)| \le Ch^\alpha.$$

We claim the following result:

Proposition 2.2. *Let $g:[0,1]\to[0,1]$ be a C^3-diffeomorphism with $g(0)=0$, $g(1)=1$. Let $N\in\mathbb{N}$, $h=1/(N+1)$. To simplify notations, we extend g as a C^3 function in a neighborhood of $[0,1]$ and for h small enough, we set*

$$h_{-1/2} = 0 - g(-h), \quad h_{N+3/2} = g((N+2)h) - 1, \quad h_j = \frac{h_{j-1/2}+h_{j+1/2}}{2}, \quad j\in\{0,N+1\}. \quad (2.4)$$

Choosing $\theta_0>0$ and for $j\in\{0,\cdots,N+1\}$,

$$\theta_j = \theta_0 + x_j, \ \text{with } x_j = g(jh). \quad (2.5)$$

we have, for $j\in\{0,\cdots,N\}$,

$$\theta_{j+1}-\theta_j = x_{j+1}-x_j = h_{j+1/2}, \quad (2.6)$$

$$h_{j+1/2}(\theta_{j+1}h_{j+1}-\theta_j h_j) = h^3 g'_{j+1/2}\left((\theta_0+g_{j+1/2})g''_{j+1/2} + (g'_{j+1/2})^2 \right) + \mathcal{O}(h^4), \quad (2.7)$$

where we have used the notations

$$g_{j+1/2} = g((j+1/2)h), \quad g'_{j+1/2} = g'((j+1/2)h), \quad g''_{j+1/2} = g''((j+1/2)h).$$

We also have, for $j\in\{1,\cdots,N\}$,

$$\frac{\theta_j h_j + \theta_{j+1}h_{j+1}}{h_{j+1/2}} - \frac{\theta_{j-1}h_{j-1}+\theta_j h_j}{h_{j-1/2}} = 2h_j + \mathcal{O}(h^2). \quad (2.8)$$

Proof. Identity (2.6) directly derives from the choice (2.5) and the notations (1.3)–(1.4).

To derive (2.7), we perform Taylor expansions:

$$\begin{cases} x_{j+1/2+\alpha/2} = g_{j+1/2} + \alpha g'_{j+1/2}\dfrac{h}{2} + \alpha^2 g''_{j+1/2}\dfrac{h^2}{8} + \mathcal{O}(h^3), & \text{for } \alpha\in\{-3,-1,1,3\}, \\ h_{j+1/2+\beta/2} = g'_{j+1/2}h + \beta g''_{j+1/2}\dfrac{h^2}{2} + \mathcal{O}(h^3), & \text{for } \beta\in\{-2,-1,0,1,2\}. \end{cases} \quad (2.9)$$

Therefore, we obtain

$$\begin{aligned}
h_{j+1/2}(\theta_{j+1}h_{j+1}-\theta_j h_j) &= h_{j+1/2}\left(\frac{\theta_j+\theta_{j+1}}{2}\right)(h_{j+1}-h_j)+h_{j+1/2}^2\left(\frac{h_j+h_{j+1}}{2}\right)\\
&= (g'_{j+1/2}h+\mathcal{O}(h^2))(\theta_0+g_{j+1/2}+\mathcal{O}(h))(g''_{j+1/2}h^2+\mathcal{O}(h^3))+(g'_{j+1/2}h+\mathcal{O}(h^2))^3\\
&= h^3 g'_{j+1/2}\left((\theta_0+g_{j+1/2})g''_{j+1/2}+(g'_{j+1/2})^2\right)+\mathcal{O}(h^4),
\end{aligned}$$

which concludes the proof of (2.7).

The proof of (2.8) can be done similarly using Taylor expansion. To begin with, we write

$$\begin{aligned}
\frac{\theta_j h_j+\theta_{j+1}h_{j+1}}{h_{j+1/2}}-\frac{\theta_{j-1}h_{j-1}+\theta_j h_j}{h_{j-1/2}} &= \theta_j\left(\frac{h_j+h_{j+1}}{h_{j+1/2}}-\frac{h_{j-1}+h_j}{h_{j-1/2}}\right)+h_{j+1}+h_{j-1}\\
&= \frac{\theta_j}{2}\left(\frac{h_{j-1/2}+h_{j+3/2}}{h_{j+1/2}}-\frac{h_{j-3/2}+h_{j+1/2}}{h_{j-1/2}}\right)+\frac{1}{2}\left(h_{j+3/2}+h_{j+1/2}+h_{j-1/2}+h_{j-3/2}\right).
\end{aligned}$$

Using the notations

$$g_j = g(jh), \quad g'_j = g'(jh), \quad g''_j = g''(jh), \tag{2.10}$$

similarly as in (2.9), Taylor expansions centered in jh yield:

$$\begin{cases}
x_{j+\alpha} = g_j+\alpha h g'_j+\alpha^2 g''_j\dfrac{h^2}{2}+\mathcal{O}(h^3), & \text{for } \alpha\in\{-2,-1,0,1,2\},\\
h_{j+\beta/2} = g'_j h+\beta g''_j\dfrac{h^2}{2}+\mathcal{O}(h^3), & \text{for } \beta\in\{-3,-1,1,3\}.
\end{cases} \tag{2.11}$$

We therefore get

$$\begin{aligned}
&h_{j+3/2}+h_{j+1/2}+h_{j-1/2}+h_{j-3/2} = 4g'_j h+\mathcal{O}(h^3) = 4h_j+\mathcal{O}(h^3),\\
&\frac{h_{j-1/2}+h_{j+3/2}}{h_{j+1/2}} = 2+\mathcal{O}(h^2), \qquad \frac{h_{j-3/2}+h_{j+1/2}}{h_{j-1/2}} = 2+\mathcal{O}(h^2),
\end{aligned}$$

so that we immediately conclude (2.8). □

2.3 Proof of Theorem 1.2

Let $g:[0,1]\to[0,1]$ be a C^3 diffeomorphism with $g(0)=0$ and $g(1)=1$, and assume that g is strictly concave on $[0,1]$. Choosing θ_j as in Proposition 2.2 with $\theta_0=\theta_g$ defined by (1.9), and using Proposition 2.1, solutions $\mathbf{u}^{h,g}$ of (1.5) satisfy

$$\begin{aligned}
&\sum_{j=1}^N h_j u'_j(t)m_j(t)\Big|_0^T+\frac{1}{2}\sum_{j=1}^N h_j\int_0^T|u'_j(t)|^2\,dt+\sum_{j=1}^N\mathcal{O}(h^2)\int_0^T|u'_j(t)|^2\,dt\\
&\quad-\frac{1}{4}\sum_{j=0}^N\int_0^T\left(h^3 g'_{j+1/2}\left((\theta_g+g_{j+1/2})g''_{j+1/2}+(g'_{j+1/2})^2\right)+\mathcal{O}(h^4)\right)\left(\frac{u'_{j+1}(t)-u'_j(t)}{h_{j+1/2}}\right)^2 dt\\
&\qquad+\frac{1}{2}\sum_{j=0}^N h_{j+1/2}\int_0^T\left(\frac{u_{j+1}(t)-u_j(t)}{h_{j+1/2}}\right)^2 dt\le\frac{1+\theta_g}{2}\int_0^T\left(\frac{u_N(t)}{h_{N+1/2}}\right)^2 dt.
\end{aligned}\tag{2.12}$$

But, by construction, θ_g satisfies

$$(\theta_g+g_{j+1/2})g''_{j+1/2}+(g'_{j+1/2})^2\le 0, \tag{2.13}$$

so that

$$-\frac{1}{4}\sum_{j=0}^{N}\int_0^T \left(h^3 g'_{j+1/2}\left((\theta_g+g_{j+1/2})g''_{j+1/2}+(g'_{j+1/2})^2\right)\right)\left(\frac{u'_{j+1}(t)-u'_j(t)}{h_{j+1/2}}\right)^2 dt \geq 0.$$

Besides, the energy $E^{h,g}(t)=E^{h,g}(\mathbf{u}^{h,g}(t),\partial_t\mathbf{u}^{h,g}(t))$ of solutions of (1.5) is preserved. Hence

$$\frac{1}{2}\sum_{j=1}^{N}h_j\int_0^T|u'_j(t)|^2\,dt+\frac{1}{2}\sum_{j=0}^{N}h_{j+1/2}\int_0^T\left(\frac{u_{j+1}(t)-u_j(t)}{h_{j+1/2}}\right)^2 dt = TE^{h,g}(\mathbf{u}^{0,h},\mathbf{u}^{1,h}).$$

We then remark that

$$\left|\sum_{j=1}^{N}\mathcal{O}(h^2)\int_0^T|u'_j(t)|^2\,dt\right|+\left|\sum_{j=0}^{N}\int_0^T\mathcal{O}(h^4)\left(\frac{u'_{j+1}(t)-u'_j(t)}{h_{j+1/2}}\right)^2 dt\right| \leq CThE^{h,g}(\mathbf{u}^{0,h},\mathbf{u}^{1,h}),$$

so that we have

$$T(1-Ch)E^{h,g}(\mathbf{u}^{0,h},\mathbf{u}^{1,h}) \leq \frac{1+\theta_g}{2}\int_0^T\left(\frac{u_N(t)}{h_{N+1/2}}\right)^2 dt-\sum_{j=1}^{N}h_ju'_j(t)m_j(t)\Big|_0^T. \tag{2.14}$$

To conclude, we only have to estimate the last term in (2.14):

$$\left|\sum_{j=1}^{N}h_ju'_j(t)m_j(t)\right| \leq \frac{1+\theta_g}{2}\left(\sum_{j=1}^{N}h_j|u'_j|^2\right)^{1/2}\left(\sum_{j=1}^{N}h_j\Big|\frac{2m_j}{\theta_j}\Big|^2\right)^{1/2}.$$

We remark that

$$\begin{aligned}\sum_{j=1}h_j\Big|\frac{2m_j}{\theta_j}\Big|^2 &= \sum_{j=1}^{N}h_j\left(\frac{u_{j+1}(t)-u_j(t)}{h_{j+1/2}}+\frac{u_j(t)-u_{j-1}(t)}{h_{j-1/2}}\right)^2 \leq 2\sum_{j=0}^{N}(h_j+h_{j+1})\left(\frac{u_{j+1}(t)-u_j(t)}{h_{j+1/2}}\right)^2\\ &\leq 4\sum_{j=0}^{N}h_{j+1/2}\left(\frac{u_{j+1}(t)-u_j(t)}{h_{j+1/2}}\right)^2+Ch^2E^{h,g}(\mathbf{u}^{0,h},\mathbf{u}^{1,h}).\end{aligned} \tag{2.15}$$

Therefore, we obtain

$$\begin{aligned}&\left|\sum_{j=1}^{N}h_ju'_j(t)m_j(t)\right|\\ &\leq(1+\theta_g)\left(\sum_{j=1}^{N}h_j|u'_j|^2\right)^{1/2}\left(\sum_{j=0}^{N}h_{j+1/2}\left(\frac{u_{j+1}(t)-u_j(t)}{h_{j+1/2}}\right)^2+Ch^2E^{h,g}(\mathbf{u}^{0,h},\mathbf{u}^{1,h})\right)^{1/2}.\\ &\leq(1+\theta_g)(1+Ch^2)E^{h,g}(\mathbf{u}^{0,h},\mathbf{u}^{1,h}).\end{aligned}$$

Plugging this last estimate in (2.14), we obtain

$$\Big(T(1-Ch)-2(1+\theta_g)(1+Ch^2)\Big)E^{h,g}(\mathbf{u}^{0,h},\mathbf{u}^{1,h}) \leq \frac{1+\theta_g}{2}\int_0^T\left(\frac{u_N(t)}{h_{N+1/2}}\right)^2 dt. \tag{2.16}$$

Therefore, for $T>T_g$, with T_g defined as in (1.10), the solutions $u^{h,g}$ of (1.5) are uniformly observable.

Remark 2.3. *Theorem 1.2 can be generalized to meshes described by strictly concave functions $g \in C^2([0,1])$ satisfying $g(0) = 0$, $g(1) = 1$ belonging to $C^{2,\alpha}([0,1])$ for some $\alpha > 0$. The proof is completely similar, except that the error terms in Proposition 2.2 should be replaced by $\mathcal{O}(h^{3+\alpha})$ in* (2.7) *and $\mathcal{O}(h^{1+\alpha})$ in* (2.8)*. Details of the proof are left to the reader.*

Remark 2.4. *In the case of a uniform mesh (corresponding to $g(x) = x$), taking $\theta_j = \theta_0 + jh$ in Proposition 2.1, one obtains ([16]):*

$$h\sum_{j=1}^{N} u_j'(t)\left(\frac{u_{j+1}(t)-u_{j-1}(t)}{2h}\right)\Bigg|_0^T + TE^{h,g(x)=x}(\mathbf{u}^{0,h},\mathbf{u}^{1,h}) + \frac{\theta_0}{2}\int_0^T \left(\frac{u_1(t)}{h}\right)^2 dt$$
$$= \frac{(1+\theta_0)}{2}\int_0^T \left(\frac{u_N(t)}{h}\right)^2 dt + \frac{h^3}{4}\sum_{j=0}^{N}\int_0^T \left(\frac{u_{j+1}'(t)-u_j'(t)}{h}\right)^2 dt. \quad (2.17)$$

The last term in the right hand side has the wrong sign and cannot be absorbed by the left hand side, even for T large. This indicates that the strict concavity condition on the diffeomorphism g assumed in Theorem 1.2 is very likely necessary to get a uniform observability result for the solutions of (1.5)*, see also Section 3.2 for further insights on this condition.*

2.4 Proof of Theorem 1.1

If g_θ is as in (1.8), one easily checks that g_θ is strictly concave, $g_\theta(0) = 0$, $g_\theta(1) = 1$, and for all $x \in [0,1]$,

$$\frac{g_\theta'(x)^2 + g_\theta(x)g_\theta''(x)}{-g_\theta''(x)} = \theta.$$

Therefore, the critical time corresponding to g_θ as in (1.8) given by Theorem 1.2 is $T_{g_\theta} = 2(1+\theta)$, so that if $\theta \in (0, T/2-1)$, $T > T_{g_\theta}$. This concludes the proof of Theorem 1.1.

Actually, the functions g_θ in (1.8) can be derived directly by observing that the leading term of the expansion in (2.7) is used in (2.13). Given g, θ_g is defined such that

$$\forall x \in [0,1], \quad (\theta_g + g(x))g''(x) + (g'(x))^2 \le 0,$$

or equivalently, in such a way that $x \mapsto (\theta_g + g(x))^2$ is concave. In particular, if we want to choose $\theta_g = \theta$ a priori, it is natural to look for g_θ with $x \mapsto (\theta + g_\theta(x))^2$ an affine function. The boundary conditions $g_\theta(0) = 0$, $g_\theta(1) = 1$ then determine the function g_θ in (1.8).

Remark 2.5. *Theorem 1.1 suggests that the critical choice $g_0(x) = \sqrt{x}$ for $x \in [0,1]$ could be well-adapted for getting uniform observability results for the corresponding solutions of* (1.5)*. However, the corresponding mesh is no more quasi-uniform as $h_{1/2}/h_{N+1/2} \simeq 2h^{-1/2}$, which goes to ∞ as $h \to 0$. We have therefore chosen to avoid that case, which would have required an additional care in the analysis close to the boundary $x = 0$.*

3 Spectral and geometric interpretations

The goal of this section is to present some insights on Theorems 1.1–1.2. In particular, we will discuss Theorem 1.1 from two complementary points of view: the spectral one, on the behavior of the eigenfunctions and the eigenvalues of the discrete Laplace operator, and the dynamical one, on the behavior of high-frequency rays.

Before going further, let us point out that the uniform mesh $g(x) = x$ can be recovered as the limit of the meshes g_θ in (1.8) when $\theta \to \infty$. It will therefore be helpful to also consider the uniform mesh

as a limiting case. In the paragraphs below, most of our discussion is valid for general diffeomorphisms g but our numerical simulations will be performed only for g of the form g_θ in (1.8) for various choices of θ to fix the ideas.

3.1 The spectral point of view

Studying spectrally the wave equation (1.1) amounts to discuss the spectrum of the Laplace operator with homogenous boundary conditions. Similarly, given a diffeomorphism $g : [0,1] \to [0,1]$ with $g(0) = g(1) = 0$, the spectral analysis of the semi-discrete wave equation (1.5) reduces to the spectral analysis of the discrete operator $A^{h,g}$ given by

$$(A^{h,g}\mathbf{u}^{h,g})_j = -\frac{1}{h_j}\Big(\frac{u^{h,g}_{j+1}-u^{h,g}_j}{h_{j+1/2}} - \frac{u^{h,g}_j - u^{h,g}_{j-1}}{h_{j-1/2}}\Big), \quad j \in \{1,\cdots,N\}, \qquad \text{with } u^{h,g}_0 = u^{h,g}_{N+1} = 0,$$

on the mesh $\mathscr{M}^{h,g}$ described by (1.3)–(1.4), which corresponds to a discretisation of the Laplacian.

The operator $A^{h,g}$ is self-adjoint and positive definite on

$$\ell^2(\mathscr{M}^{h,g}) = \{\mathbf{u}^{h,g} \text{ defined on } \mathscr{M}^{h,g} \text{ with } u^{h,g}_0 = u^{h,g}_{N+1} = 0\}$$
$$\text{endowed with the norm } \big\|\mathbf{u}^{h,g}\big\|^2_{\ell^2(\mathscr{M}^{h,g})} = \sum_{j=1}^N h_j |u^{h,g}_j|^2. \quad (3.1)$$

In particular, we have the identity

$$\langle A^{h,g}\mathbf{u}^{h,g}, \mathbf{v}^{h,g}\rangle_{\ell^2(\mathscr{M}^{h,g})} = \sum_{j=0}^N h_{j+1/2}\left(\frac{u^{h,g}_{j+1}-u^{h,g}_j}{h_{j+1/2}}\right)\left(\frac{v^{h,g}_{j+1}-v^{h,g}_j}{h_{j+1/2}}\right).$$

Therefore, $\ell^2(\mathscr{M}^{h,g})$ admits a basis of eigenfunctions $\mathbf{w}^{k,h,g}$ ($k \in \{1,\cdots,N\}$) of $A^{h,g}$ with corresponding eigenvalues $\lambda^{k,h,g}$ such that $0 < \lambda^{1,h,g} \le \cdots \le \lambda^{N,h,g}$. The spectral problem reads:

$$\begin{cases} -\Big(\dfrac{w^k_{j+1}-w^k_j}{h_{j+1/2}} - \dfrac{w^k_j - w^k_{j-1}}{h_{j-1/2}}\Big) = \lambda^k h_j w^k_j, \quad j \in \{1,\cdots,N\}, \\ w^k_0 = w^k_{N+1} = 0. \end{cases} \quad (3.2)$$

One then immediately deduces that each eigenvalue is simple[1].

The usual strategy to study the observability problem (1.7) is based on the use of Fourier series expansions and Ingham type inequalities. The observability inequality (1.7) turns out to be, roughly, equivalent to the following two spectral properties:

- A *uniform observability property for all the eigenvectors* $\mathbf{w}^{k,h,g}$, uniform with respect to the mesh size. In our setting, this property would read as follows: there exists a constant $C > 0$ such that for all $N \in \mathbb{N}$ (corresponding to $h = 1/(N+1)$), for all $k \in \{1,\cdots,N\}$, the eigenvectors $\mathbf{w}^{k,h,g}$ satisfy
$$\lambda^{k,h,g}\big\|\mathbf{w}^{k,h,g}\big\|^2_{\ell^2(\mathscr{M}^{h,g})} \le C\left(\frac{w^{k,h,g}_N}{h_{N+1/2}}\right)^2. \quad (3.3)$$

[1]Indeed, if we have two different eigenvectors $\mathbf{w}^{h,g}, \tilde{\mathbf{w}}^{h,g}$ corresponding to the same eigenvalue, we can find $\alpha \in \mathbb{R}$ such that $w^{h,g}_1 - \alpha\tilde{w}^{h,g}_1 = 0$. As $w^{h,g}_0 - \alpha\tilde{w}^{h,g}_0 = 0$, using the equation at $j = 1$ we obtain $w^{h,g}_2 - \alpha\tilde{w}^{h,g}_2 = 0$ and so forth, so that $\mathbf{w}^{h,g} = \alpha\tilde{\mathbf{w}}^{h,g}$.

- A *uniform gap condition on the eigenvalues*, i.e.

$$\liminf_{N\to\infty} \inf_{1\le k\le N-1} \left\{ \sqrt{\lambda^{k+1,h,g}} - \sqrt{\lambda^{k,h,g}} \right\} > 0. \tag{3.4}$$

Indeed, if both properties (3.3) and (3.4) are satisfied, then Ingham's Lemma [17] applies and yields the uniform observability property (1.7) in any time $T > T_{g,Ing}$ with

$$T_{g,Ing} = \frac{2\pi}{\gamma_{h,g,as}}, \tag{3.5}$$

$\gamma_{h,g,as}$ being the asymptotic gap[2], i.e.

$$\gamma_{h,g,as} = \inf_{K\in\mathbb{N}} \liminf_{N\to\infty} \inf_{K\le k\le N-1} \left\{ \sqrt{\lambda^{k+1,h,g}} - \sqrt{\lambda^{k,h,g}} \right\} > 0. \tag{3.6}$$

When $g : [0,1] \to [0,1]$ is a C^3 diffeomorphism which is strictly concave and satisfies $g(0) = 0$, $g(1) = 1$, the uniform observability property (3.3) can be derived using a multiplier technique on the spectral system (3.2). But it can be derived directly from the estimate (2.16) applied to $\mathbf{u}^{h,g}(t) = \exp(i\sqrt{\lambda^{k,h,g}}t)\mathbf{w}^{k,h,g}$, dividing the corresponding estimate by T and passing to the limit $T \to \infty$.

However, the uniform gap condition (3.4) seems more delicate to obtain, as this would require a careful description of the eigenvalues. As the mesh is non-uniform, this seems very intricate. In fact, to our knowledge, the only case in which a spectral gap was proven for non-uniform meshes corresponds to the case of the $1d$ wave equation (1.1) discretized in space using the mixed finite element method, see [7].

We can nevertheless perform a numerical investigation of both properties (3.3) and (3.4). We restrict ourselves to diffeomorphisms g of the form g_θ as in (1.8) for various choices of $\theta > 0$ to fix the ideas.

In Figures 1–3, we plot the eigenvectors $\mathbf{w}^{k,h,g}$ corresponding to g_θ in (1.8) for $\theta = 0.1$, $\theta = 1$, $\theta = 10$ and compare them with the eigenvectors $\mathbf{w}^{k,h,g}$ corresponding to the uniform case $g(x) = x$ (in that case, $\mathbf{w}^{k,h,g}$ is explicit and equals $(\sqrt{2}\sin(k\pi jh))_{j\in\{1,\cdots,N\}}$) for various values of k. Several comments are in order. The first eigenvectors nearly coincide, whatever the choice of g is, since they correspond to low frequencies and are therefore close to the eigenvectors of the continuous Laplace operator on $(0,1)$ - which are simply of the form $\sqrt{2}\sin(k\pi x)$. For large k, an interesting phenomenon appears. Though the eigenvectors corresponding to a uniform mesh are still equidistributed, the k-th eigenvectors corresponding to the strictly concave meshes $\mathscr{M}^{g_\theta,h}$ become more and more localized close to $x = 1$ when k increases, and this is more and more the case when θ decreases. As expected, this indicates that the eigenvectors corresponding to large eigenvalues are localized in the part of the domain in which the mesh is the finest, and this phenomenon is amplified when the ratio between the coarsest mesh and the finest one grows, as

$$\frac{\sup_j h_{j+1/2}}{\inf_j h_{j+1/2}} = \frac{h_{1/2}}{h_{N+1/2}} \underset{h\to 0}{\simeq} \frac{g'_\theta(0)}{g'_\theta(1)} = 1 + \frac{1}{\theta}.$$

In Figure 4, we plot the dispersion diagrams, i.e. the graph $k \to \sqrt{\lambda^{k,h,g}}$ corresponding to g_θ in (1.8) with $\theta = 0$, $\theta = 0.1$, $\theta = 1$, $\theta = 10$ and compare them with the one corresponding to the case of a uniform mesh, given by $k \to \frac{2}{h}\sin\left(\frac{k\pi h}{2}\right)$. One easily sees that the dispersion diagrams corresponding

[2]The time needed by Ingham's inequality is determined by the asymptotic gap, but the constants in the inequality also depend on the minimal gap of the whole sequence, and also on how fast the sequence approximates the asymptotic gap ([21]). But with our definition of the asymptotic gap, as the bottom of the discrete spectra converges to the bottom of the spectrum of the continuous Laplacian, these low-frequency part will not yield any difficulty.

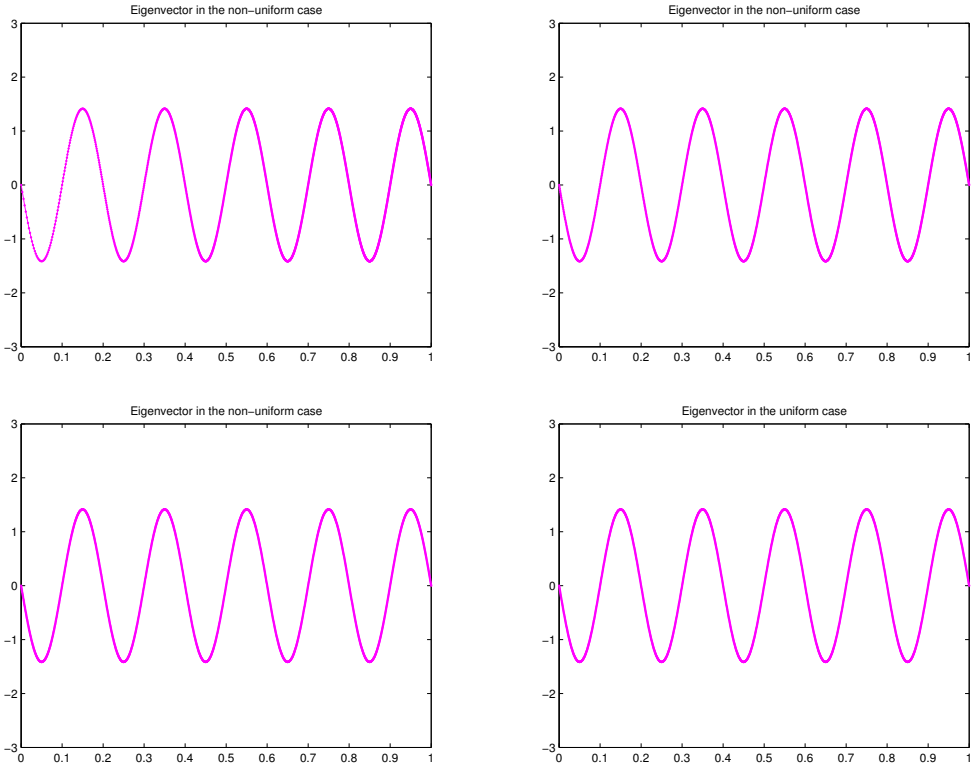

Figure 1: Plot of the eigenvectors $\mathbf{w}^{k,h,g}$ for $k = 10$, $N = 2000$, and various functions g: from left to right and top to bottom, $g = g_{0.1}$, $g = g_1$, $g = g_{10}$ and $g(x) = x$.

to the mesh g_θ in (1.8) do not present any horizontal tangent, contrarily to the case of a uniform mesh. Therefore, the corresponding spectral gaps

$$\inf_{1\le k\le N-1}\left\{\sqrt{\lambda^{k+1,h,g}}-\sqrt{\lambda^{k,h,g}}\right\}$$

for g_θ in (1.8) should be bounded away from 0. In Table 1, we report the computations of the spectral gap for various values of N. We remark that the spectral gap seems to be independent of the number of points for the meshes corresponding to g_θ, while it goes very rapidly to zero in the case of a uniform mesh. If we employ the gap computed numerically for the largest N to estimate the time $T_{g,Ing}$ in (3.5) by $T_{g,Ing,est}$ given by

$$T_{g,Ing,est} = \frac{2\pi}{\inf_{1\le k\le N-1}\left\{\sqrt{\lambda^{k+1,h,g}}-\sqrt{\lambda^{k,h,g}}\right\}}, \tag{3.7}$$

we get a rather good agreement with the time predicted by (1.10) at least for small θ. However, the estimated time $T_{g,Ing,est}$ in (3.7), which appear to be close to $T_{g,Ing}$ in (3.5) in our experiments as the spectral gap concerns the high-frequency part of the spectrum, seems to be significantly better than the one in (1.10) for θ of the order of 1. Whether $T_{g,Ing}$ is the sharp critical time for the uniform observability property (1.7) for (1.5) is an open problem.

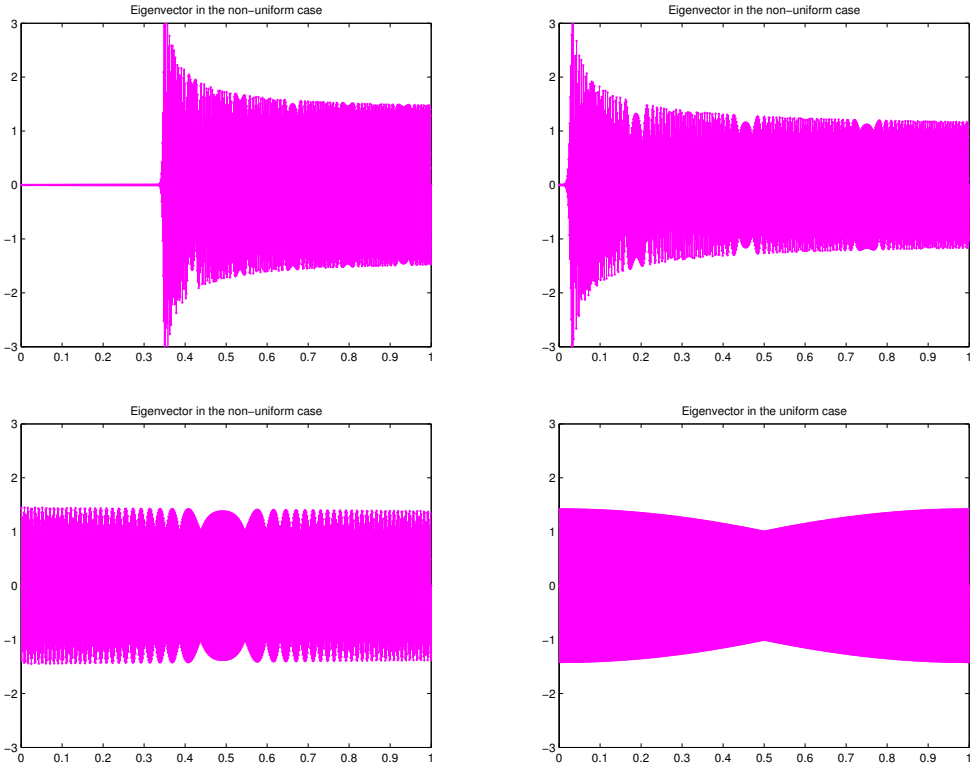

Figure 2: Plot of the eigenvectors $\mathbf{w}^{k,h,g}$ for $k = 1000$, $N = 2000$, and various functions g: from left to right and top to bottom, $g = g_{0.1}$, $g = g_1$, $g = g_{10}$ and $g(x) = x$.

3.2 A dynamical system approach

We now discuss the observability of the discrete wave equation (1.5) from the point of view of the propagation properties of discrete bicharacteristic rays, which is the cornerstone of the analysis of the observability properties of the continuous wave equation (1.1) in any space dimension, leading to the so-called *Geometric Control Condition* (GCC) [1, 2].

Rays of geometric optics are defined as the projections on the physical space (t, x) of the bicharacteristic rays given by the Hamiltonian corresponding to the principal part of the operator. In the case of the classical wave equation with unit velocity, the Hamiltonian is simply

$$H_c(t, x, \tau, \xi) = -\tau^2 + |\xi|^2, \tag{3.8}$$

and the bicharacteristic rays are given by the curves $s \mapsto (t(s), x(s), \tau(s), \xi(s))$ solving

$$\left\{ \begin{array}{l} \dfrac{dt}{ds} = \partial_\tau H_c(t(s), x(s), \tau(s), \xi(s)) = -2\tau(s), \\ \dfrac{dx}{ds} = \nabla_\xi H_c(t(s), x(s), \tau(s), \xi(s)) = 2\xi(s), \end{array} \right. \quad \left\{ \begin{array}{l} \dfrac{d\tau}{ds} = -\partial_t H_c(t(s), x(s), \tau(s), \xi(s)) = 0, \\ \dfrac{d\xi}{ds} = -\nabla_x H_c(t(s), x(s), \tau(s), \xi(s)) = 0, \end{array} \right. \tag{3.9}$$

for an initial data belonging to the characteristic set, i.e. satisfying $H_c(t(s_0), x(s_0), \tau(s_0), \xi(s_0)) = 0$. This is so while the curve does not hit the boundary of the domain, where a reflection law has to be

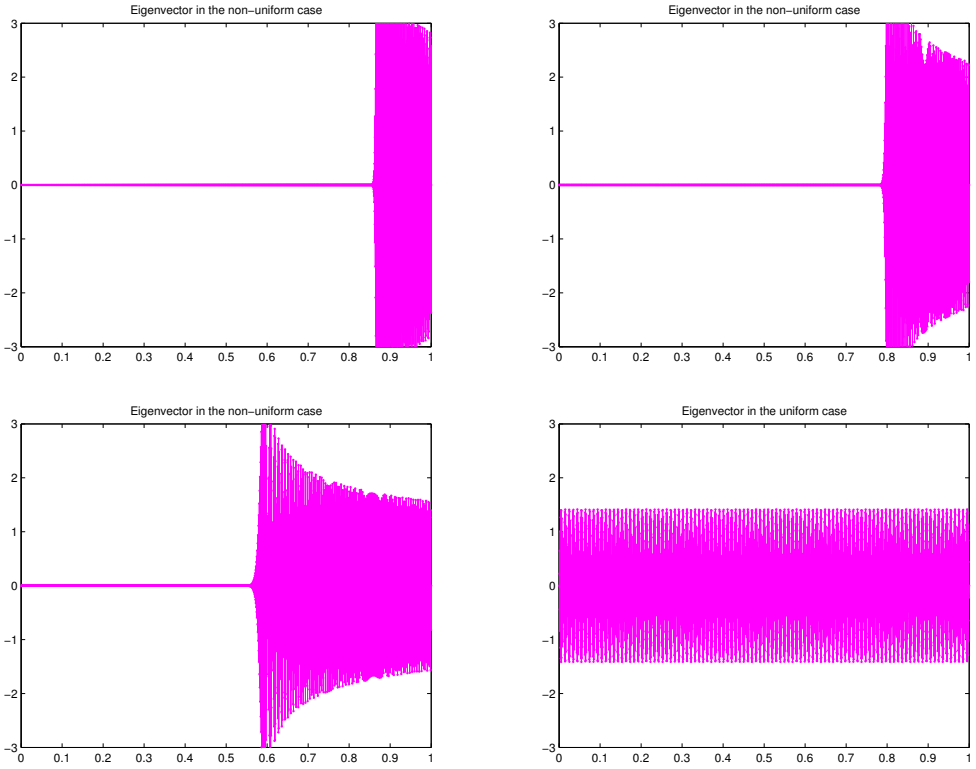

Figure 3: Plot of the eigenvectors $\mathbf{w}^{k,h,g}$ for $k = 1900$, $N = 2000$, and various functions g: from left to right and top to bottom, $g = g_{0.1}$, $g = g_1$, $g = g_{10}$ and $g(x) = x$.

prescribed, the Descartes-Snell's law. Thus, the projections on the physical space of these rays simply are straight lines traveling at velocity one inside the domain Ω. The construction given in [25] yield solutions of the wave equation which are localized in an arbitrary small neighborhood of these rays.

When discretizing the wave equation, the situation is more intricate. One needs to derive carefully a discrete counterpart of the Hamiltonian and the corresponding bicharacteristics by means of the discrete Fourier transform. This was done in [19] for the discrete wave equation in an infinite lattice (i.e. with no boundary) and, more recently, this theory was extended to non-uniform meshes obtained by means of a C^2 diffeomorphism (not necessarily concave) of the uniform mesh $(jh)_{j\in\mathbb{Z}}$ in [20].

To be more precise, in [20], solutions of (1.5) were constructed, with frequencies of the order of $1/h$, localized around the rays of geometric optics given by the projection on the physical space of the bicharacteristic curves provided by the Hamiltonian

$$H(t,x,\tau,\xi) = -g'(x)\tau^2 + \frac{4}{g'(x)}\sin\left(\frac{\xi}{2}\right)^2, \tag{3.10}$$

or equivalently

$$H(t,x,\tau,\xi) = -\tau^2 + c(x)\omega(\xi)^2, \text{ with } c(x) = \frac{1}{g'(x)^2}, \quad \omega(\xi) = 2\sin\left(\frac{\xi}{2}\right). \tag{3.11}$$

The bicharacteristic rays corresponding to that Hamiltonian are now more intricate as the Fourier

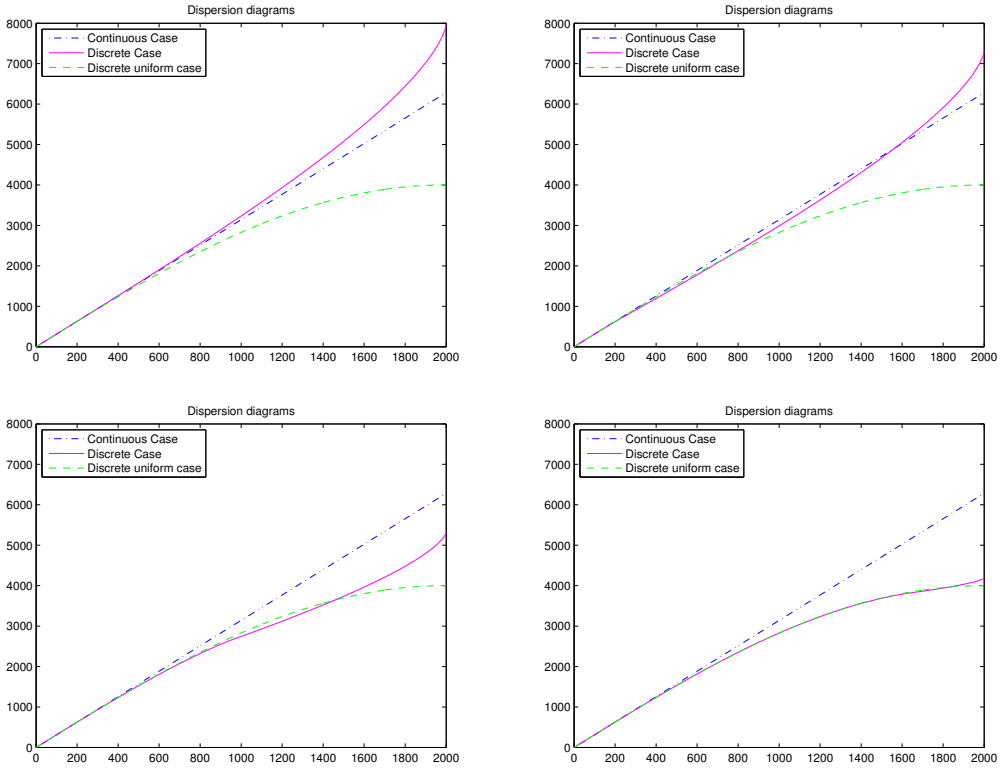

Figure 4: Dispersion diagram $k \to \sqrt{\lambda^{k,h,g}}$ for various g: from left to right and top to bottom, $g = g_0$, $g = g_{0.1}$, $g = g_1$, $g = g_{10}$. The corresponding dispersion diagrams are plotted in magenta plain line, the dispersion diagram $k \mapsto k\pi$ corresponding to the continuous Laplace operator is plotted in blue dashed line and the dispersion diagram $k \mapsto 2\sin(k\pi h/2)/h$ is plotted in green dotted line.

variable ξ may evolve in time:

$$\begin{cases} \dfrac{dt}{ds}(s) = \partial_\tau H(t(s), x(s), \tau(s), \xi(s)) = -2\tau(s), \\ \dfrac{dx}{ds}(s) = \nabla_\xi H(t(s), x(s), \tau(s), \xi(s)) = 2c(x(s))\omega(\xi(s))\partial_\xi \omega(\xi(s)), \\ \dfrac{d\tau}{ds}(s) = -\partial_t H(t(s), x(s), \tau(s), \xi(s)) = 0, \\ \dfrac{d\xi}{ds}(s) = -\nabla_x H(t(s), x(s), \tau(s), \xi(s)) = -\partial_x c(x(s))\omega(\xi(s))^2, \end{cases} \tag{3.12}$$

with an initial condition at $s = 0$ given by $(t_0, x_0, \tau_0, \xi_0)$ satisfying $H(t_0, x_0, \tau_0, \xi_0) = 0$.

To better understand the dynamics of the bicharacteristic rays, remark that for all s, $\tau(s) = \tau_0$. Besides, for all s, $H(t(s), x(s), \tau(s), \xi(s)) = 0$, so that for all s,

$$\tau_0^2 = c(x(s))\omega(\xi(s))^2.$$

Now, as dt/ds does not vanish, we can parametrize the curve $s \mapsto (t(s), x(s), \tau(s), \xi(s))$ by $t \mapsto$

$(t, x(t), \tau_0, \xi(t))$, and we obtain

$$\left\{ \begin{array}{c} \dfrac{dx}{dt}(t) = -\dfrac{1}{\tau_0} c(x(t))\omega(\xi(t))\partial_\xi\omega(\xi(t)), \qquad \dfrac{d\xi}{dt}(t) = \dfrac{1}{2\tau_0}\partial_x c(x(t))\omega(\xi(t))^2, \\ \tau_0^2 = c(x(t))\omega(\xi(t))^2. \end{array} \right. \tag{3.13}$$

This yields in particular

$$\begin{aligned} \frac{d^2x}{dt^2}(t) &= -\frac{1}{\tau_0}\partial_x c(x(t))\frac{dx}{dt}(t)\omega(\xi(t))\partial_\xi\omega(\xi(t)) - \frac{1}{\tau_0}c(x(t))\left((\partial_\xi\omega(\xi(t)))^2 + \omega(\xi(t))\partial_{\xi\xi}\omega(\xi(t))\right)\frac{d\xi}{dt}(t) \\ &= \frac{1}{2\tau_0^2}c(x(t))\partial_x c(x(t))\omega(\xi(t))^2\left(2(\partial_\xi\omega(\xi(t)))^2 - \left((\partial_\xi\omega(\xi(t)))^2 + \omega(\xi(t))\partial_{\xi\xi}\omega(\xi(t))\right)\right) \\ &= \frac{1}{2}\partial_x c(x(t))\left((\partial_\xi\omega(\xi(t)))^2 - \omega(\xi(t))\partial_{\xi\xi}\omega(\xi(t))\right). \end{aligned}$$

With c and ω as in (3.11), we therefore obtain that for all t,

$$\frac{d^2x}{dt^2}(t) = \frac{1}{2}\,\frac{d}{dx}\left(\frac{1}{(\partial_x g)^2}\right)\Big|_{x=x(t)} = -\frac{g''(x(t))}{g'(x(t))^3}. \tag{3.14}$$

Therefore, in the part of the domain in which g is strictly concave, the corresponding rays are curved in the direction of increasing x. This gives a complementary interpretation of the strict concavity assumption on g in Theorem 1.2.

Note that the above computation of d^2x/dt^2 indicates that the curvature of the rays of geometric optics is driven by the product of the signs of $\partial_x c(x)$ and of $(\partial_\xi\omega(\xi))^2 - \omega(\xi)\partial_{\xi\xi}\omega(\xi)$.

This later quantity is constant equal to one in the case of $\omega(\xi) = 1$ (the continuous case) and in the case of $\omega(\xi) = 2\sin(\xi/2)$ corresponding to the finite difference case we are considering. Though, in the continuous case, the rays cannot turn without hitting the boundary. Indeed, thanks to (3.13),

$$\left|\frac{dx}{dt}(t)\right| = \frac{1}{|\tau_0|}c(x(t))|\omega(\xi(t))\partial_\xi\omega(\xi(t))| = \sqrt{c(x(t)}|\partial_\xi\omega(\xi(t))|,$$

so that the velocity of rays can vanish only if $\partial_\xi\omega$ vanishes for some ξ. When $\omega(\xi) = \xi$, i.e. in the continuous setting, this cannot happen, while when $\omega(\xi) = 2\sin(\xi/2)$, $\partial_\xi\omega(\xi) = \cos(\xi/2)$ vanishes for $\xi = \pm\pi$.

For the mesh corresponding to g_θ as in (1.8), the rays are all curved towards $x = 1$, and this curvature is more important when θ is small. In fact, formula (3.14) easily provides that the rays traveling on a mesh $\mathscr{M}^{h,g}$ for $g = g_\theta$ as in (1.8) satisfy

$$\frac{d^2x}{dt^2}(t) = \frac{2}{1+2\theta}. \tag{3.15}$$

To illustrate this result, we plot in Figure 5 the absolute value of the solutions of the discrete wave equation (1.5) in meshes $\mathscr{M}^{h,g}$ for various choices of g corresponding to an initial data given by

$$\left\{ \begin{array}{l} u_j^0 = \exp\left(-\dfrac{(jh-1/2)^2}{h}\right)\exp\left(\dfrac{ig(jh)\xi_0}{h}\right), \\ u_j^1 = \exp\left(-\dfrac{(jh-1/2)^2}{h}\right)\exp\left(\dfrac{ig(jh)\xi_0}{h}\right)\dfrac{2i\sin(\xi_0/2)}{h_j}, \end{array} \right. \tag{3.16}$$

in the spirit of the Gaussian beams [25]. The oscillatory term localizes the solution in frequency in a neighborhood of ξ_0/h. This oscillatory term is modulated by a Gaussian envelope centered in a neighborhood of size $\simeq 1/\sqrt{h}$ of $x = 1/2$.

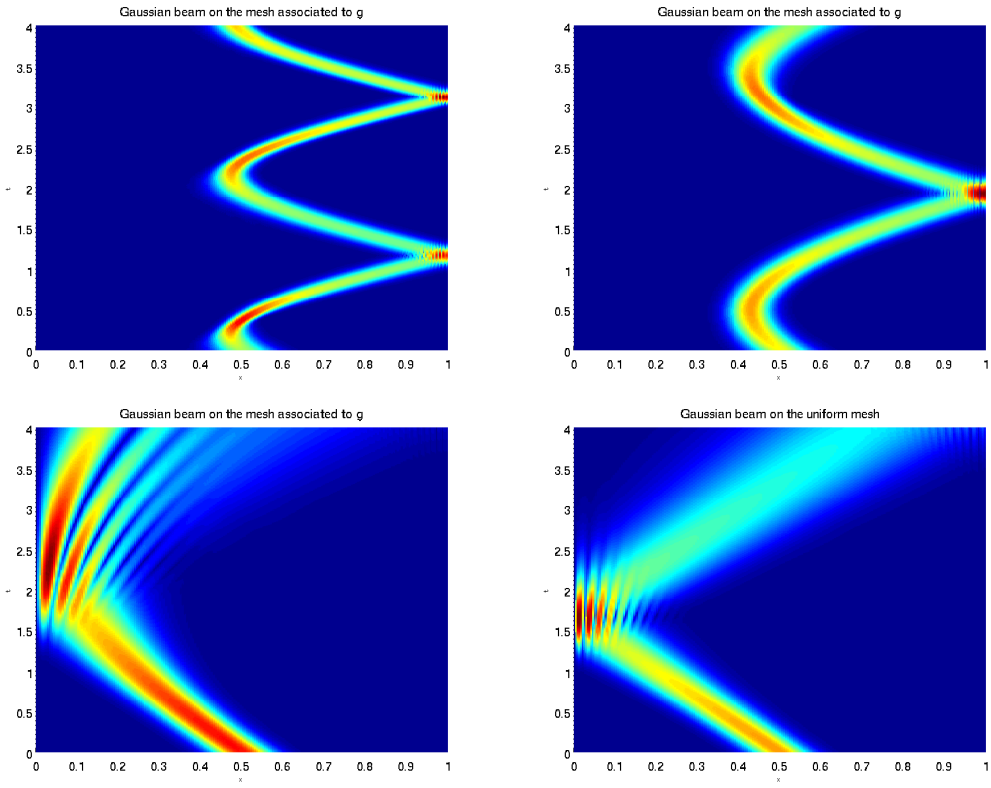

Figure 5: Solutions of (1.5) with the initial data $(u^{0,h}, u^{1,h})$ as in (3.16) for various choices of g, with $N = 200$, $\xi_0 = 0.8\pi$. From left to right and top to bottom, $g = g_{0,1}$, $g = g_1$, $g = g_{10}$ and $g = g(x)$. The abscissa represents the space variable $x \in (0, 1)$ and the ordinate is the time variable $t \in (0, 4)$.

In the uniform case, the ray simply is a straight line except when it hits the boundary. But its velocity does not correspond to the velocity 1 of the continuous wave equation (1.1). Actually, the equation (3.13) immediately yields in the case of a uniform mesh that, away from the boundary, $\xi(t) = \xi_0$ for all t and thus

$$\left|\frac{dx}{dt}\right| = |\partial_\xi \omega(\xi)| = \cos\left(\frac{\xi_0}{2}\right).$$

Therefore, taking ξ_0 close to π provides rays that travel arbitrarily slowly, making the observability property to blow up in the case of a uniform mesh.

In Figure 5, we see that when θ decreases, the corresponding ray is more and more bent to the right, as formula (3.15) shows.

We may also use this analysis to derive estimates on the characteristic time for the uniform observability property (1.7) for (1.5). Indeed, similarly as in the continuous case [2], we may infer that the critical time for the uniform observability property (1.7) is given by the longest characteristic ray that does not meet the observation set $x = 1$.

We therefore display on Figure 6 the phase portraits (x, ξ) corresponding to the dynamical system (3.13) (with the choice $\tau_0 > 0$ which can be done without loss of generality) for the functions $g = g_\theta$ in (1.8) for $\theta \in \{0.1, 1, 10\}$ and in the uniform case $g(x) = x$.

On the boundary $x = 0$, we conjecture that the reflection occurs with the law $\xi \to 2\pi - \xi$, in agreement with the usual Descartes Snell's law, corresponding to the constraint $H(t, x, \tau, \xi) = 0$.

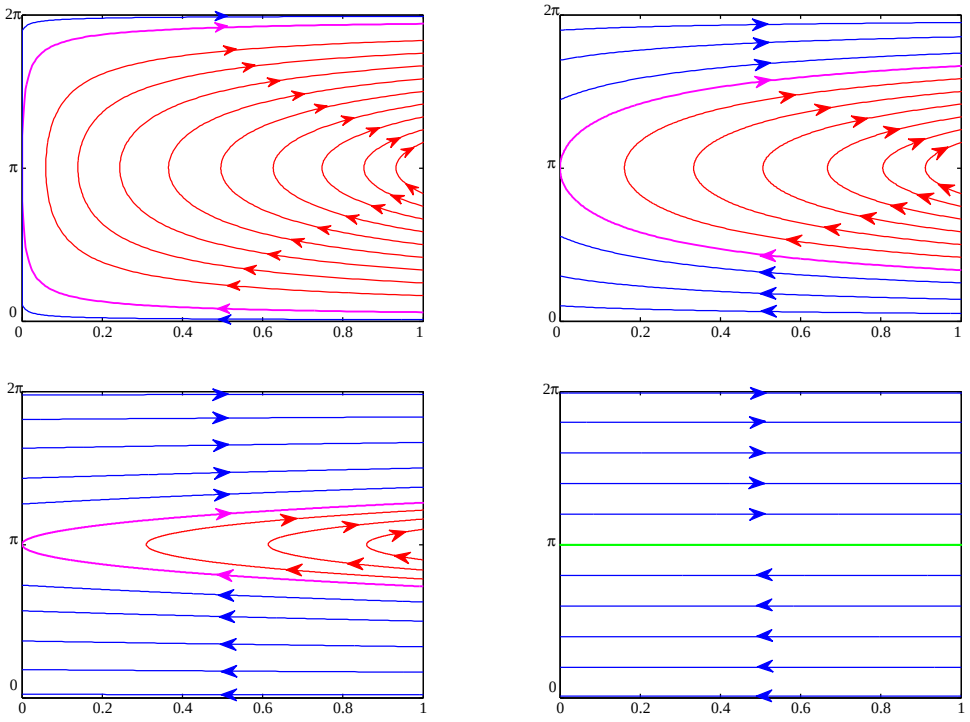

Figure 6: Phase portraits for various functions g: from left to right and top to bottom, $g = g_{0.1}$, $g = g_1$, $g = g_{10}$ and $g(x) = x$. In blue/magenta/red, we represent trajectories reflecting transversally/diffractively/internally at the left endpoint and transversally at the right endpoint of the interval. In green, the fixed points of the dynamical system for the case of the uniform mesh, $g(x) = x$.

We now compute the length of the longest characteristic ray which does not meet the observation set $x = 1$. It is obvious that we may restrict ourselves to the characteristics starting with a negative velocity at $x_0 = 1$ so that we also impose $\xi_0 \in (0, \pi]$. Then three cases occur:
• the "blue" case: In some time t_1, the ray hits the boundary $x = 0$, is then reflected according to Descartes Snell's law, and goes back to $x = 1$. It corresponds to the trajectories in blue in Figure 6.
• the "magenta" case: The ray reflects diffractively a the boundary $x = 0$ and goes back to $x = 1$. This corresponds to the (unique) trajectory in magenta in Figure 6.
• the "red" case: The ray does not hit the boundary $x = 0$ and is bent to $x = 1$. This corresponds to the trajectories in red in Figure 6.
Each case is characterized by the initial frequency parameter ξ_0. In order to determine the critical value ξ^* which determines each case, we focus on the magenta curve. As it is characterized by the fact that at $x = 0$, its velocity vanishes, which occurs only for $\xi = \pi$, we must have

$$c(0)\omega(\pi)^2 = c(1)\omega(\xi^*)^2, \quad \text{i.e.} \quad \xi^* = 2\arcsin\left(\frac{g'(1)}{g'(0)}\right). \tag{3.17}$$

Consequently, the blue case is characterized by $\xi_0 \in (0, \xi^*)$, the critical case by $\xi_0 = \xi^*$, and the red case by $\xi_0 \in (\xi^*, \pi]$.

The blue case $\xi_0 \in (0, \xi^*)$. In this case, $t \mapsto x(t)$ starts by decreasing during a time interval $(0, t_1)$ and hits the boundary at time $t_1(\xi_0)^-$ corresponding to $(x, \xi) = (0, \xi_1)$ with

$$\xi_1 = 2 \arcsin\left(\frac{g'(1)}{g'(0)} \sin\left(\frac{\xi_0}{2}\right)\right), \text{ given by the relation } c(0)\omega(\xi_1)^2 = c(1)\omega(\xi_0)^2.$$

At time $t_1(\xi_0)^+$, the characteristic ray starts from $(x, \xi) = (0, 2\pi - \xi_1)$ and goes right until the time $t_2(\xi_0)$ in which it hits the boundary $x = 1$. Based on the the relation $dx = (\partial_t x)dt$ along the trajectory, the total time spent by the characteristic ray starting from $(1, \xi_0)$ to reach the boundary $x = 1$ is then given by

$$T_b(\xi_0) = t_2(\xi_0) = \int_0^{t_1(\xi_0)} dt + \int_{t_1(\xi_0)}^{t_2(\xi_0)} dt = \int_0^1 \frac{dx}{|\partial_t x|} + \int_0^1 \frac{dx}{|\partial_t x|} = 2\int_0^1 \frac{dx}{\sqrt{c(x)}|\partial_\xi \omega(\xi)|}.$$

Using that along the trajectory

$$c(x)\omega(\xi)^2 = c(1)\omega(\xi_0)^2, \text{ and } c(x) = \frac{1}{g'(x)^2},$$

we obtain that, along the ray,

$$|\partial_\xi \omega(\xi)| = \sqrt{1 - \left(\frac{g'(x)}{g'(1)} \sin\left(\frac{\xi_0}{2}\right)\right)^2},$$

so that

$$T_b(\xi_0) = 2\int_0^1 \frac{g'(x)\,dx}{|\partial_\xi \omega(\xi)|} = 2\int_0^1 \frac{g'(x)\,dx}{\sqrt{1 - \left(\frac{g'(x)}{g'(1)} \sin\left(\frac{\xi_0}{2}\right)\right)^2}}.$$

This quantity is obviously an increasing function of ξ_0. We therefore obtain that the characteristic time corresponding to the rays in the blue region is

$$T_b = \sup_{\xi_0 \in (0,\xi^*)} T_b(\xi_0) = 2\int_0^1 \frac{g'(x)\,dx}{\sqrt{1 - \left(\frac{g'(x)}{g'(1)} \sin\left(\frac{\xi^*}{2}\right)\right)^2}} = 2\int_0^1 \frac{g'(x)\,dx}{\sqrt{1 - \left(\frac{g'(x)}{g'(0)}\right)^2}}. \tag{3.18}$$

The red case $\xi_0 \in (\xi^*, \pi]$. When $\xi_0 \in (\xi^*, \pi]$, the ray does not hit the boundary $x = 0$ and its velocity $\partial_t x$ changes of sign at some time $t_1(\xi_0)$. At this time, we necessarily have $\xi(t_1(\xi_0)) = \pi$ which corresponds to the only possibility to cancel the velocity, so that the rays turns at the point $x_1 = x(t_1(\xi_0))$ given by the relation

$$\sqrt{c(x_1)}\omega(\pi) = \sqrt{c(1)}\omega(\xi_0), \quad i.e. \quad g'(x_1) = \frac{g'(1)}{\sin\left(\frac{\xi_0}{2}\right)}.$$

Similar computations as in the blue case yield

$$T_r(\xi_0) = 2\int_{x_1}^1 \frac{g'(x)\,dx}{\sqrt{1 - \left(\frac{g'(x)}{g'(1)} \sin\left(\frac{\xi_0}{2}\right)\right)^2}} = 2\int_{x_1}^1 \frac{g'(x)\,dx}{\sqrt{1 - \left(\frac{g'(x)}{g'(x_1)}\right)^2}}.$$

The magenta case $\xi_0 = \xi^*$. This case can be recovered as a limit of the blue case or of the red case and therefore does not need any further analysis.

Guess on the characteristic time. Based on the analysis above, we expect that the critical time for the uniform observability property (1.7) for (1.5) for a given strictly concave function g is given by

$$T_{g,char} = 2 \sup_{x_1 \in [0,1]} \left\{ \int_{x_1}^1 \frac{g'(x)\,dx}{\sqrt{1 - \left(\frac{g'(x)}{g'(x_1)}\right)^2}} \right\}. \tag{3.19}$$

But so far, this is still an open issue.

Actually, it is not straightforward from the above formula in (3.19) that the time $T_{g,char}$ in (3.19) is smaller than the time T_g in (1.10) for strictly concave functions g as in Theorem 1.2. It is not even clear for which $x_1 \in (0,1]$ this supremum is achieved for general strictly concave functions g.

Though, according to [20, Theorem 3.5], we can show that the time of uniform observability for (1.5) is necessarily larger than the time $T_{g,char}$ in (3.19): Otherwise, one could construct a sequence of discrete rays localized around one ray of the discrete Hamiltonian (3.13) which does not touch the boundary $x = 0$ and violating the uniformity of the discrete observability inequality (1.7).

To support our above conclusions, let us focus again on the case $g = g_\theta$ in (1.8), in which case explicit computations can be done:

$$\int_{x_1}^1 \frac{g'(x)\,dx}{\sqrt{1 - \left(\frac{g'(x)}{g'(x_1)}\right)^2}} = 2\sqrt{2\theta+1}\sqrt{1-x_1}.$$

so that

$$T_{g_\theta,char} = 2\sqrt{2\theta+1}, \tag{3.20}$$

which is indeed strictly smaller than $T_{g_\theta} = 2(1+2\theta)$ in (1.10) for $\theta > 0$ as claimed above. We report the corresponding values in Table 1. As one easily checks, the values given by (3.20) are very close to the ones given by the estimated Ingham time $T_{g,Ing,est}$ in (3.7), thus supporting the idea that both times coincide with the sharp critical time needed for the uniform observability (1.7) for (1.5).

N	g_0	$g_{0.1}$	g_1	g_{10}	$g(x) = x$
500	3.1133	2.8780	1.837	0.7004	0.0148
1000	3.1213	2.8739	1.8247	0.6950	0.0074
2000	3.1272	2.8716	1.8208	0.6917	0.0037
$T_{g,Ing,est}$ in (3.7)	2.01	2.19	3.45	9.08	∞
T_g in (1.10)	"2"	2.2	4	22	∞
$T_{g,char}$ in (3.20)	"2"	2.19	3.46	9.17	∞

Table 1: Spectral gaps for the meshes $\mathscr{M}^{h,g}$ for $g = g_0$, $g = g_{0.1}$, $g = g_1$, $g = g_{10}$ and $g(x) = x$, and for various values of N and estimated times $T_{g,Ing,est}$ given by (3.7) for uniform observability and the characteristic time $T_{g,char}$ in (3.20) provided by micro-local analysis.

4 The controllability problem

In this section, we illustrate the interest of the observability property for controllability purposes.

4.1 The continuous setting

In the continuous case, the controllability problem corresponding to the observability property (1.2) for (1.1) is the following: Given $(y^0, y^1) \in L^2(0,1) \times H^{-1}(0,1)$, find a control function $v \in L^2(0,T)$ such that the solution y of

$$\begin{cases} \partial_{tt} y - \partial_{xx} y = 0, & (t,x) \in (0,T) \times (0,1), \\ y(t,0) = 0,\ y(t,1) = v(t), & t \in (0,T), \\ y(0,x) = y^0(x),\ \partial_t y(0,x) = y^1(x), & x \in (0,1), \end{cases} \tag{4.1}$$

satisfies the controllability requirement

$$(y(T,x), \partial_t y(T,x)) = (0,0), \quad x \in (0,1). \tag{4.2}$$

Thanks to the linearity and the time-reversibility of the wave equation (4.1), this controllability property is equivalent to the a priori more general one: Given $(y^0, y^1) \in L^2(0,1) \times H^{-1}(0,1)$ and $(y_f^0, y_f^1) \in L^2(0,1) \times H^{-1}(0,1)$, find a control function $v \in L^2(0,T)$ such that the solution y of (4.1) satisfies

$$(y(T,x), \partial_t y(T,x)) = (y_f^0, y_f^1), \quad x \in (0,1). \tag{4.3}$$

Let us focus on the controllability problem (4.1)–(4.2) and briefly recall how it can be solved by using the observability property (1.2) for (1.1). Following [18] and the modified Hilbert Uniqueness Method (HUM) proposed in [10], for $T > 2$ we first choose a smooth function $\eta : [0,T] \to [0,1]$ flat at $t = 0$ and at $t = T$ and equals to 1 on a sufficiently large interval of time so that the following observability inequality is satisfied for all u solving (1.1) with initial data $(u^0, u^1) \in H_0^1(0,1) \times L^2(0,1)$:

$$\left\| (u^0, u^1) \right\|^2_{H_0^1(0,1) \times L^2(0,1)} \leq C_{obs}^2 \int_0^T \eta(t) |\partial_x u(t,1)|^2 \, dt. \tag{4.4}$$

Then, given $(y^0, y^1) \in L^2(0,1) \times H^{-1}(0,1)$, we introduce the functional J defined by

$$J(u^0, u^1) = \frac{1}{2} \int_0^T \eta(t) |\partial_x u(t,1)|^2 \, dt + \int_0^1 y^0 u^1 - \langle y^1, u^0 \rangle_{H^{-1}, H^1}, \tag{4.5}$$

where u denotes the solution of (1.1) with initial data $(u^0, u^1) \in H_0^1(0,1) \times L^2(0,1)$, and $\langle \cdot, \cdot \rangle_{H^{-1}, H^1}$ denotes the duality product between $H^{-1}(0,1)$ and $H_0^1(0,1)$ given by

$$\langle y^1, u^0 \rangle_{H^{-1}, H^1} = \int_0^1 \partial_x ((-\partial_{xx}^d)^{-1} y^1) \partial_x u^0,$$

where $(-\partial_{xx}^d)^{-1}$ denotes the inverse of the Laplace operator on $(0,1)$ with homogeneous Dirichlet boundary conditions.

Thanks to the observability property (4.4) for solutions of (1.1), one easily checks that the functional J is coercive and strictly convex on $H_0^1(0,1) \times L^2(0,1)$. Therefore, it admits a unique minimizer $(U^0, U^1) \in H_0^1(0,1) \times L^2(0,1)$. If we denote by U the corresponding solution of (1.1), one obtains that, setting

$$v(t) = \eta(t) \partial_x U(t,1), \quad t \in (0,T), \tag{4.6}$$

the solution y of (4.1) with initial datum (y^0, y^1) and control function v as in (4.6) satisfies the control requirement (4.2). Besides, the control v in (4.6) is the one of minimal $L^2(0,T; dt/\eta)$-norm.

Remark that the classical HUM method ([18]) uses $\eta(t) = 1$ for all $t \in (0,T)$, but the method above presents the advantage of ensuring regular controls for regular data and therefore performs better when adapted numerically, see [10, 11].

4.2 The discrete setting

When trying to compute an approximation of the discrete control v given by (4.6) associated to an initial datum (y^0, y^1), the basic idea is to take a discrete approximation $(\mathbf{y}^{0,h}, \mathbf{y}^{1,h})$ of (y^0, y^1) and then to compute the minimizer of a discrete counterpart J^h of the functional J in (4.5), namely

$$J^h(\mathbf{u}^{0,h}, \mathbf{u}^{1,h}) = \frac{1}{2}\int_0^T \eta(t)\left|\frac{u_N^h(t)}{h_{N+1/2}}\right|^2 dt + \sum_{j=1}^N h_j y_j^{0,h} u_j^{1,h} - \sum_{j=1}^N h_j y_j^{1,h} u_j^{0,h}, \tag{4.7}$$

where $\mathbf{u}^h$ denotes the solution of (1.5) with initial datum $(\mathbf{u}^{0,h}, \mathbf{u}^{1,h})$. If a minimizer $(\mathbf{U}^{0,h}, \mathbf{U}^{1,h})$ is found, one may expect that

$$v^h(t) = -\eta(t)\frac{U_N^h(t)}{h_{N+1/2}}, \quad t \in (0,T), \tag{4.8}$$

would produce a good approximation of v in (4.6). To support that idea, we could also remark that the function v^h obtained that way solves the following discrete controllability problem: the solution $\mathbf{y}^h$ of

$$\begin{cases} h_j y_j''(t) - \Big(\dfrac{y_{j+1}(t)-y_j(t)}{h_{j+1/2}} - \dfrac{y_j(t)-y_{j-1}(t)}{h_{j-1/2}}\Big) = 0, & t \in (0,T),\ 1 \le j \le N, \\ y_0(t) = 0,\ y_{N+1}(t) = v^h(t), & t \in (0,T), \\ y_j(0) = y_j^{0,h},\ y_j'(0) = y_j^{1,h}, & 1 \le j \le N, \end{cases} \tag{4.9}$$

satisfies

$$(y_j(T), \partial_t y_j(T)) = (0,0), \quad j \in \{1, \cdots, N\}, \tag{4.10}$$

that is a discrete version of the controllability problem (4.1)–(4.2).

But this process may fail to converge as J^h may not be uniformly coercive with respect to h. Actually, even worse, as a consequence of Banach Steinhaus theorem, one can show that if the discrete systems (1.5) are not uniformly observable, then there exists initial data in $L^2(0,1) \times H^{-1}(0,1)$ such that the sequence of corresponding discrete controls v^h in (4.8) is unbounded as $h \to 0$, see [10, Theorem 8]. It turns out that in the case of a uniform mesh, that is when $g(x) = x$, uniform observability fails [16]. Therefore the above process, based on the minimization of J^h in (4.7), may create divergent sequences of controls. This is due to the fact that uniform meshes generate spurious high-frequency solutions that propagate arbitrarily slowly, recall Section 3.2. To recover uniform observability properties on a uniform mesh, high-frequency components need to be filtered ([12, 14]), either by Fourier ([16]), bi-grid techniques ([24]), or Tychonoff regularization ones ([28]).

As a consequence of the analysis of the present paper, a new remedy can be designed based on the use of the non-uniform grids that we introduce here. Indeed, as a consequence of Theorems 1.1–1.2, minimizing the corresponding discrete analogs of the functionals J above, the obtained discrete controls v^h in (4.8) are bounded. Basic convergence arguments show that, provided $(\mathbf{y}^{0,h}, \mathbf{y}^{1,h})$ converge to (y^0, y^1) in a suitable sense, the discrete controls v^h in (4.8) converge to the control v in (4.6). One can also derive additional rates of convergence if we assume (y^0, y^1) to be slightly smoother than $L^2(0,1) \times H^{-1}(0,1)$. We refer to [10, 11] for further developments on these issues.

To illustrate these ideas and facts, we perform some numerical experiments. We choose an initial datum (y^0, y^1) to be controlled and a natural sequence of corresponding discrete approximations $(y^{0,h}, y^{1,h})$. For $T > 2$ fixed, we choose $\theta = (T-2)/2$ and a mesh described by g_θ as in (1.8). We then compute v^h as in (4.8) for this mesh. As initial datum (y^0, y^1) we choose the ones in Figure 7. In Figure 8, left, we plot the control v_h computed on the mesh $\mathscr{M}^{g_\theta,h}$ with $\theta = (T-2)/2$, $T = 4$ and $h = 1/301$. In the case of a uniform mesh, the computation of the minimizer of J^h does not converge due to a bad conditioning of the functional [22]. Therefore, to compare the control v_h computed on the mesh $\mathscr{M}^{g_\theta,h}$, we plot in Figure 8, right, the controls obtained in time $T = 4$ on a uniform mesh

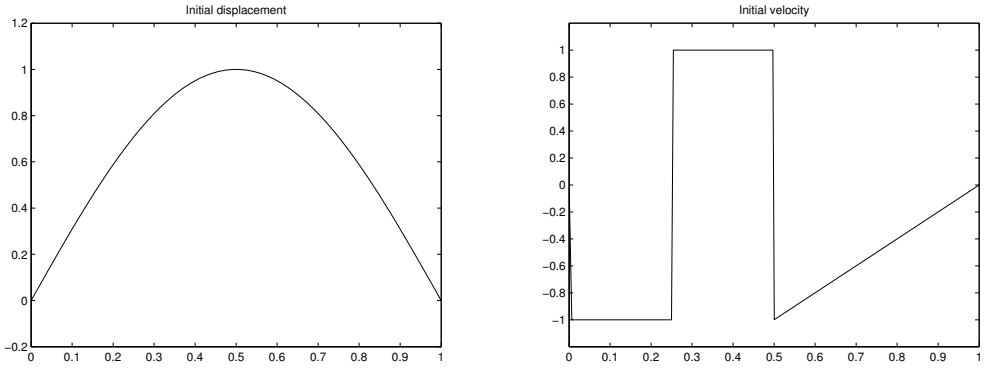

Figure 7: Initial datum to be controlled: left, the initial displacement y^0, right, the initial velocity y^1.

using the filtering mechanism of [16] which simply consists on minimizing the functional J^h in (4.7) on the subspace $(V^h(\gamma))^2$ for some $\gamma < 4$, where $V^h(\gamma)$ is defined by

$$V^h(\gamma) = \text{Span}\left\{ (\sin(k\pi jh))_{1\le j\le N} \Big| \, k \ge 1 \text{ with } \frac{4}{h^2}\sin\left(\frac{k\pi h}{2}\right)^2 \le \frac{\gamma}{h^2} \right\}.$$

Minimizing J^h on $(V^h(\gamma))^2$ yields a minimizer $(\mathbf{U}^{0,h,\gamma}, \mathbf{U}^{1,h,\gamma})$, and if $\mathbf{U}^{h,\gamma}$ denotes the corresponding solution of (1.5),

$$v^{h,\gamma}(t) = -\eta(t)\frac{U_N^{h,\gamma}(t)}{h_{N+1/2}}, \quad t \in (0,T), \tag{4.11}$$

is the corresponding filtered control. This filtered control is proved to converge in $L^2(0,T)$ to the corresponding control (4.6) in [16], see aso [10].

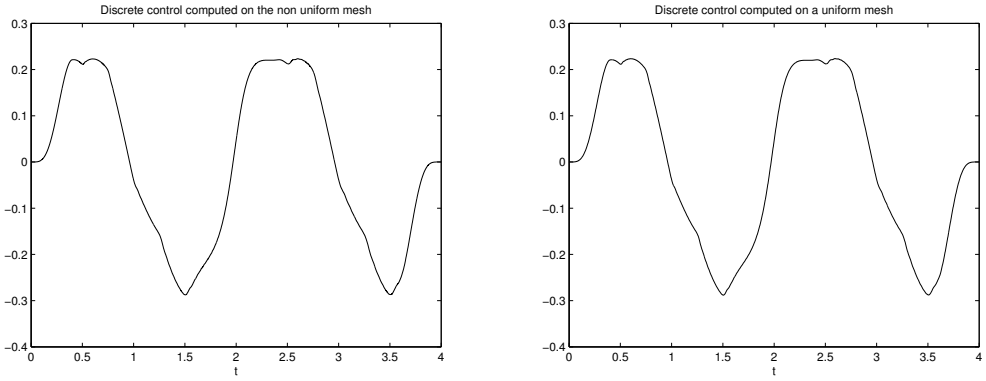

Figure 8: Discrete controls. Left, the control given by v^h in (4.8) computed on the mesh $\mathscr{M}^{g_\theta,h}$ with $\theta = (T-2)/2$, $T = 4$ and $h = 1/301$. Right, the control $v^{h,\gamma}$ in (4.11) computed on a uniform mesh with $\gamma = 1$, $T = 4$, $h = 1/301$.

Figure 8 shows that the controls v^h and $v^{h,\gamma}$ look exactly the same, therefore supporting the idea

that choosing the mesh suitably as in this paper, one does not further need of any filtering process to recover the convergence of the discrete controls.

5 Finite element approximations

This section aims at extending our approach to the study of uniform observability properties of the space semi-discrete wave equation discretized using the finite element method.

5.1 Statements and results

Finite element methods for the approximation of the wave equations are based on the variational formulation of (1.1): Find $u(t,\cdot) \in H_0^1(0,1)$ such that

$$\begin{cases} \dfrac{d^2}{dt^2}(u(t,\cdot),\varphi)_{L^2(0,1)} + (\partial_x u(t,\cdot),\partial_x\varphi)_{L^2(0,1)} = 0, \quad \forall \varphi \in H_0^1(0,1),\ \forall t \in (0,T), \\ (u(0,\cdot),\partial_t u(0,\cdot)) = (u^0,u^1). \end{cases} \tag{5.1}$$

Let g be a smooth diffeomorphism of the interval $[0,1]$ with $g(0)=0$ and $g(1)=1$. We introduce the mesh $\mathscr{M}^{h,g}$ as in (1.3)–(1.4), and the corresponding P_1 finite element space

$$H_0^{1,h,g}(0,1) = \big\{ f^h \in C^0([0,1]),\ f^h(0) = f^h(1) = 0\ , \\ \text{and } f^h \text{ is affine in each interval } [x_j,x_{j+1}],\ j \in \{0,\cdots,N\} \big\}.$$

The P_1 finite element approximation of (5.1) then reads as follows: Find $u^h(t,\cdot) \in H_0^{1,h,g}(0,1)$ such that

$$\begin{cases} \dfrac{d^2}{dt^2}(u^h(t,\cdot),\varphi^h)_{L^2(0,1)} + (\partial_x u^h(t,\cdot),\partial_x\varphi^h)_{L^2(0,1)} = 0, \quad \forall \varphi^h \in H_0^{1,h,g}(0,1),\ \forall t \in (0,T), \\ (u^h(0,\cdot),\partial_t u^h(0,\cdot)) = (u^{h,0},u^{h,1}). \end{cases} \tag{5.2}$$

As $H_0^{1,h,g}(0,1)$ is a finite dimensional space spanned by the "hat" functions

$$\phi_j(x) = \frac{x-x_{j-1}}{h_{j-1/2}} 1_{(x_{j-1},x]}(x) + \frac{x_{j+1}-x}{h_{j+1/2}} 1_{(x_j,x_{j+1}]}(x),$$

we look for u^h solution of (5.2) under the form

$$u^h(t,x) = \sum_{k=1}^{N} u_k(t)\phi_k(x).$$

We then easily obtain that the vector of coefficients $\mathbf{u}^h(t) = (u_j(t))_{0\le j\le N+1}$ satisfies the following second-order linear ODE system:

$$\begin{cases} \dfrac{h_{j+1/2}}{6}u_{j+1}''(t) + \dfrac{2h_j}{3}u_j''(t) + \dfrac{h_{j-1/2}}{6}u_{j-1}''(t) - \Big(\dfrac{u_{j+1}(t)-u_j(t)}{h_{j+1/2}} - \dfrac{u_j(t)-u_{j-1}(t)}{h_{j-1/2}}\Big) = 0, \\ \qquad\qquad (t,j) \in (0,T)\times\{1,\cdots,N\}, \\ u_0(t) = u_{N+1}(t) = 0, \qquad t \in (0,T), \\ (u_j(0),u_j'(0)) = (u_j^0,u_j^1), \qquad j \in \{1,\cdots,N\}. \end{cases} \tag{5.3}$$

The total energy for the solutions of (5.2), equivalently (5.3), given by

$$E_f^{h,g}(\mathbf{u}^h(t),\partial_t\mathbf{u}^h(t)) := \frac{1}{2}\sum_{j=0}^{N}\int_{x_j}^{x_{j+1}}(|\partial_t u^h(t,x)|^2+|\partial_x u^h(t,x)|^2)\,dx$$
$$= \frac{1}{12}\sum_{j=0}^{N}h_{j+1/2}|u'_{j+1}(t)+u'_j(t)|^2+\frac{1}{6}\sum_{j=1}^{N}h_j|u'_j(t)|^2+\frac{1}{2}\sum_{j=0}^{N}h_{j+1/2}\Big|\frac{u_{j+1}(t)-u_j(t)}{h_{j+1/2}}\Big|^2, \quad (5.4)$$

is time independent.

Focusing on the observability inequality with an observation through $x=1$, we get the following counterpart to Theorem 1.2:

Theorem 5.1. *Let $g:[0,1]\to[0,1]$ be a $C^3([0,1])$ diffeomorphism satisfying $g(0)=0$, $g(1)=1$, and assume that g is strictly concave. Set θ_g as in (1.9). Then, for any $T>T_g$ as in (1.10), the space semi-discrete equations (5.3) are uniformly observable through $x=1$ in the following sense: There exist $h^\star>0$ and a constant $C^g_{obs}>0$ (independent of h) such that for all $h\in(0,h^\star)$, the solutions $\mathbf{u}^{h,g}$ of (5.3) on the mesh $\mathscr{M}^{h,g}$ satisfy the observability inequality:*

$$E_f^{h,g}(\mathbf{u}^{0,h},\mathbf{u}^{1,h})\le (C^g_{obs})^2\left(\int_0^T\left|\frac{u_N^g(t)}{h_{N+1/2}}\right|^2dt+\int_0^T|(u_N^g)'(t)|^2\,dt\right). \quad (5.5)$$

The discrete observability inequality in (5.5) involves a reinforcement of the observation operator $u_N^g(t)/h_{N+1/2}$ corresponding to the spatial derivative $\partial_x u(t,1)$ by the term $(u_N^g)'(t)$. However, such discrete uniform observability inequality (5.5) allows to recover the observability inequality (1.2) when passing to the limit $h\to 0$. Besides, this reinforcement of the discrete observability inequality is still localized close to $x=1$, so that we can still interpret (5.5) as a discrete observability inequality through $x=1$.

As in the context of finite differences, one can immediately deduce from Theorem 5.1 the following counterpart of Theorem 1.1:

Theorem 5.2. *For any $T>2$, there exists a smooth diffeomorphism g such that the solutions $\mathbf{u}^{h,g}$ of (5.3) are uniformly observable through $x=1$ in time T. Such g can be chosen explicitly of the form g_θ as in (1.8) for $\theta\in(0,T/2-1)$.*

The proof of Theorem 5.2 is omitted as it is a straightforward consequence of Theorem 5.1. In Section 5.2 below, we present the proof of Theorem 5.1. It is based on the same strategy as the one in Section 2, though the proofs are more technically involved.

Before going further, let us mention that the insights given in Section 3 for the finite difference method are completely similar for the finite element method. From a spectral point of view, the eigenvectors corresponding to high eigenvalues concentrate close to the set where the mesh is refined, similarly to Figures 1–2–3, and numerical evidences show that the eigenvalues enjoy a uniform gap condition when the mesh transformation is strictly concave. From a dynamical point of view, the computation of the dynamics of the rays can still be done but with a more intricate dispersion relation ω, and one can construct Gaussian beam solutions curved towards the set in which the mesh is finer as in Figure 5.

5.2 Proof of Theorem 5.1

Similarly as in Section 2, we start with a multiplier identity:

Proposition 5.3 (A discrete multiplier identity)**.** *If* $\mathbf{u}^h(t)$ *solves* (5.3) *and* $\mathbf{m}^h(t)$ *denotes the multiplier in* (2.1)*, we have the following identity:*

$$\begin{aligned}
&\sum_{j=1}^{N}\Big(\frac{h_{j+1/2}}{6}u'_{j+1}(t)+\frac{2h_j}{3}u'_j(t)+\frac{h_{j-1/2}}{6}u'_{j-1}(t)\Big)m_j(t)\Big|_0^T\\
&+\frac{1}{24}\sum_{j=1}^{N}\int_0^T\Big[\theta_{j+1}\Big(\frac{3h_{j+3/2}}{h_{j+1/2}}-1\Big)+3\theta_j\Big(\frac{h_{j-1/2}}{h_{j+1/2}}-\frac{h_{j+1/2}}{h_{j-1/2}}\Big)-\theta_{j-1}\Big(\frac{3h_{j-3/2}}{h_{j-1/2}}-1\Big)\Big]|u'_j(t)|^2\,dt\\
&+\frac{1}{12}\sum_{j=0}^{N}\int_0^T(\theta_{j+1}-\theta_j)|u'_{j+1}(t)+u'_j(t)|^2\,dt+\frac{1}{2}\sum_{j=0}^{N}\int_0^T(\theta_{j+1}\ -\theta_j)\left|\frac{u_{j+1}(t)-u_j(t)}{h_{j+1/2}}\right|^2dt\\
&+\frac{1}{24}\sum_{j=1}^{N}\int_0^T\theta_j\Big(\frac{h_{j-1/2}}{h_{j+1/2}}-\frac{h_{j+1/2}}{h_{j-1/2}}\Big)|u'_{j+1}(t)-u'_{j-1}(t)|^2\,dt\\
&-\frac{1}{24}\sum_{j=0}^{N}\int_0^T\Big[\theta_{j+1}\Big(\frac{h_{j+1/2}}{h_{j+3/2}}+\frac{2h_{j+3/2}}{h_{j+1/2}}-1\Big)+\theta_j\Big(1-\frac{2h_{j-1/2}}{h_{j+1/2}}-\frac{h_{j+1/2}}{h_{j-1/2}}\Big)\Big]|u'_{j+1}(t)-u'_j(t)|^2\,dt\\
&+\frac{\theta_0}{24}\Big(\frac{h_{-1/2}}{h_{1/2}}-\frac{h_{1/2}}{h_{-1/2}}\Big)\int_0^T|u'_1(t)|^2\,dt+\frac{\theta_{N+1}}{24}\Big(\frac{h_{N+1/2}}{h_{N+3/2}}-\frac{h_{N+3/2}}{h_{N+1/2}}\Big)\int_0^T|u'_N(t)|^2\,dt\\
&+\frac{\theta_0}{12}\int_0^T|u'_1(t)|^2\,dt+\frac{\theta_0}{2}\int_0^T\left|\frac{u_1(t)}{h_{1/2}}\right|^2dt=\frac{\theta_{N+1}}{12}\int_0^T|u'_N(t)|^2\,dt+\frac{\theta_{N+1}}{2}\int_0^T\left|\frac{u_N(t)}{h_{N+1/2}}\right|^2dt,\quad(5.6)
\end{aligned}$$

where $h_{-1/2}$ *and* $h_{N+3/2}$ *can be set arbitrarily.*

Proof. We use the multiplier $\mathbf{m}^h$ in (2.1): we multiply the equation (5.3) by m_j, sum on $j\in\{1,\cdots,N\}$ and integrate in time to obtain

$$A_f-B_f=0,\ \text{with}\ A_f=\sum_{j=1}^{N}\int_0^T\Big(\frac{h_{j+1/2}}{6}u''_{j+1}(t)+\frac{2h_j}{3}u''_j(t)+\frac{h_{j-1/2}}{6}u''_{j-1}(t)\Big)m_j(t)\,dt$$
$$\text{and}\ \ B_f=\sum_{j=1}^{N}\int_0^T\Big(\frac{u_{j+1}(t)-u_j(t)}{h_{j+1/2}}-\frac{u_j(t)-u_{j-1}(t)}{h_{j-1/2}}\Big)m_j(t)\,dt.$$

The term B_f coincides with B in the finite difference case and we refer to (2.3) for its computation.

We thus focus on the computation of the term A_f. By integration by parts in time, we get

$$A_f=\sum_{j=1}^{N}\Big(\frac{h_{j+1/2}}{6}u'_{j+1}(t)+\frac{2h_j}{3}u'_j(t)+\frac{h_{j-1/2}}{6}u'_{j-1}(t)\Big)m_j(t)\Big|_0^T-A_f^0$$
$$\text{with}\ \ A_f^0=-\sum_{j=1}^{N}\int_0^T\Big(\frac{h_{j+1/2}}{6}u'_{j+1}(t)+\frac{2h_j}{3}u'_j(t)+\frac{h_{j-1/2}}{6}u'_{j-1}(t)\Big)m'_j(t)\,dt.$$

We now put the term in A_f^0 in a suitable form:

$$\Big(\frac{h_{j+1/2}}{6}u'_{j+1}+\frac{2h_j}{3}u'_j+\frac{h_{j-1/2}}{6}u'_{j-1}\Big)m'_j=\frac{\theta_j}{12}a_j$$
$$\text{with}\ \ a_j=\big(h_{j+1/2}u'_{j+1}+4h_ju'_j+h_{j-1/2}u'_{j-1}\big)\left(\frac{u'_{j+1}-u'_j}{h_{j+1/2}}+\frac{u'_j-u'_{j-1}}{h_{j-1/2}}\right).$$

Using

$$h_{j+1/2}u'_{j+1} + 4h_j u'_j + h_{j-1/2}u'_{j-1} = h_{j+1/2}(u'_{j+1} + u'_j) + h_{j-1/2}(u'_j + u'_{j-1}) + 2h_j u'_j,$$
$$\frac{u'_{j+1} - u'_j}{h_{j+1/2}} + \frac{u'_j - u'_{j-1}}{h_{j-1/2}} = \frac{u'_{j+1} + u'_j}{h_{j+1/2}} - \frac{u'_j + u'_{j-1}}{h_{j-1/2}} - 2\left(\frac{1}{h_{j+1/2}} - \frac{1}{h_{j-1/2}}\right)u'_j,$$

we derive

$$\begin{aligned} a_j =& \Big((u'_{j+1} + u'_j)^2 - (u'_j + u'_{j-1})^2\Big) + (u'_{j+1} + u'_j)(u'_j + u'_{j-1})\left(\frac{h_{j-1/2}}{h_{j+1/2}} - \frac{h_{j+1/2}}{h_{j-1/2}}\right) \\ &- 2u'_j\left(\frac{1}{h_{j+1/2}} - \frac{1}{h_{j-1/2}}\right)\left(h_{j+1/2}(u'_{j+1} + u'_j) + h_{j-1/2}(u'_j + u'_{j-1})\right) \\ &+ 2h_j u'_j\left(\frac{u'_{j+1} - u'_j}{h_{j+1/2}} + \frac{u'_j - u'_{j-1}}{h_{j-1/2}}\right). \end{aligned}$$

By discrete integration by parts, the first term will yield a term in $|u'_{j+1} + u'_j|^2$, so we leave it under that form for the moment.

We write the other terms in terms of u'_j and differences of the form $u'_{j+1} - u'_j$ and $u'_j - u'_{j-1}$ only. We thus write

$$\begin{aligned} (u'_{j+1} + u'_j)(u'_j + u'_{j-1}) = -\frac{1}{2}\left(|u'_{j+1} - u'_{j-1}|^2 - |u'_{j+1} - u'_j|^2 - |u'_j - u'_{j-1}|^2\right) \\ + 2u'_j(u'_{j+1} - u'_j) - 2u'_j(u'_j - u'_{j-1}) + 4|u'_j|^2, \end{aligned}$$

and

$$u'_j\left(h_{j+1/2}(u'_{j+1} + u'_j) + h_{j-1/2}(u'_j + u'_{j-1})\right) = h_{j+1/2}u'_j(u'_{j+1} - u'_j) - h_{j-1/2}u'_j(u'_j - u'_{j-1}) + 4h_j|u'_j|^2.$$

so that a_j becomes

$$\begin{aligned} a_j =& \Big((u'_{j+1} + u'_j)^2 - (u'_j + u'_{j-1})^2\Big) + |u'_j|^2\left(4\left(\frac{h_{j-1/2}}{h_{j+1/2}} - \frac{h_{j+1/2}}{h_{j-1/2}}\right) - 8h_j\left(\frac{1}{h_{j+1/2}} - \frac{1}{h_{j-1/2}}\right)\right) \\ &- \frac{1}{2}\left(\frac{h_{j-1/2}}{h_{j+1/2}} - \frac{h_{j+1/2}}{h_{j-1/2}}\right)\left(|u'_{j+1} - u'_{j-1}|^2 - |u'_{j+1} - u'_j|^2 - |u'_j - u'_{j-1}|^2\right) \\ &+ u'_j(u'_{j+1} - u'_j)\left(2\left(\frac{h_{j-1/2}}{h_{j+1/2}} - \frac{h_{j+1/2}}{h_{j-1/2}}\right) - 2\left(\frac{1}{h_{j+1/2}} - \frac{1}{h_{j-1/2}}\right)h_{j+1/2} + 2\frac{h_j}{h_{j+1/2}}\right) \\ &+ u'_j(u'_j - u'_{j-1})\left(-2\left(\frac{h_{j-1/2}}{h_{j+1/2}} - \frac{h_{j+1/2}}{h_{j-1/2}}\right) + 2\left(\frac{1}{h_{j+1/2}} - \frac{1}{h_{j-1/2}}\right)h_{j-1/2} + 2\frac{h_j}{h_{j-1/2}}\right) \\ =& \Big((u'_{j+1} + u'_j)^2 - (u'_j + u'_{j-1})^2\Big) \\ &- \frac{1}{2}\left(\frac{h_{j-1/2}}{h_{j+1/2}} - \frac{h_{j+1/2}}{h_{j-1/2}}\right)\left(|u'_{j+1} - u'_{j-1}|^2 - |u'_{j+1} - u'_j|^2 - |u'_j - u'_{j-1}|^2\right) \\ &+ u'_j(u'_{j+1} - u'_j)\left(3\frac{h_{j-1/2}}{h_{j+1/2}} - 1\right) + u'_j(u'_j - u'_{j-1})\left(3\frac{h_{j+1/2}}{h_{j-1/2}} - 1\right). \end{aligned}$$

Using this last identity, we derive

$$A_f^0 = A_f^1 + A_f^2 + A_f^3 + A_f^4 \text{ with}$$

$$A_f^1 = \frac{1}{12}\sum_{j=1}^{N}\int_0^T \theta_j\big(|u'_{j+1}(t)+u'_j(t)|^2 - |u'_j(t)+u'_{j-1}(t)|^2\big)\,dt,$$

$$A_f^2 = -\frac{1}{24}\sum_{j=1}^{N}\int_0^T \theta_j\left(\frac{h_{j-1/2}}{h_{j+1/2}} - \frac{h_{j+1/2}}{h_{j-1/2}}\right)|u'_{j+1}-u'_{j-1}|^2\,dt,$$

$$A_f^3 = \frac{1}{24}\sum_{j=1}^{N}\int_0^T \theta_j\left(\frac{h_{j-1/2}}{h_{j+1/2}} - \frac{h_{j+1/2}}{h_{j-1/2}}\right)\big(|u'_{j+1}-u'_j|^2 + |u'_j-u'_{j-1}|^2\big)\,dt,$$

$$A_f^4 = \frac{1}{12}\sum_{j=1}^{N}\int_0^T \theta_j\left(u'_j(u'_{j+1}-u'_j)\left(3\frac{h_{j-1/2}}{h_{j+1/2}}-1\right) + u'_j(u'_j-u'_{j-1})\left(3\frac{h_{j+1/2}}{h_{j-1/2}}-1\right)\right)dt.$$

Computation of A_f^1:

$$A_f^1 = \frac{\theta_{N+1}}{12}\int_0^T |u'_N(t)|^2\,dt - \frac{\theta_0}{12}\int_0^T |u'_1(t)|^2\,dt - \frac{1}{12}\sum_{j=0}^{N}\int_0^T (\theta_{j+1}-\theta_j)|u'_{j+1}(t)+u'_j(t)|^2\,dt.$$

The term A_f^2 does not require any further computation.
Computation of A_f^3:

$$\begin{aligned}A_f^3 = \frac{1}{24}\sum_{j=0}^{N}\int_0^T \Big[\theta_{j+1}\Big(\frac{h_{j+1/2}}{h_{j+3/2}} - \frac{h_{j+3/2}}{h_{j+1/2}}\Big) + \theta_j\Big(\frac{h_{j-1/2}}{h_{j+1/2}} - \frac{h_{j+1/2}}{h_{j-1/2}}\Big)\Big]|u'_{j+1}(t)-u'_j(t)|^2\,dt \\ - \frac{\theta_0}{24}\Big(\frac{h_{-1/2}}{h_{1/2}} - \frac{h_{1/2}}{h_{-1/2}}\Big)\int_0^T |u'_1(t)|^2\,dt - \frac{\theta_{N+1}}{24}\Big(\frac{h_{N+1/2}}{h_{N+3/2}} - \frac{h_{N+3/2}}{h_{N+1/2}}\Big)\int_0^T |u'_N(t)|^2\,dt,\end{aligned}$$

Computation of A_f^4:

$$\begin{aligned}A_f^4 =& \frac{1}{12}\sum_{j=0}^{N}\int_0^T \Big[\theta_{j+1}\Big(\frac{3h_{j+3/2}}{h_{j+1/2}}-1\Big)u'_{j+1}(t) + \theta_j\Big(\frac{3h_{j-1/2}}{h_{j+1/2}}-1\Big)u'_j(t)\Big](u'_{j+1}(t)-u'_j(t))\,dt \\ =& \frac{1}{24}\sum_{j=0}^{N}\int_0^T \Big[\theta_{j+1}\Big(\frac{3h_{j+3/2}}{h_{j+1/2}}-1\Big) - \theta_j\Big(\frac{3h_{j-1/2}}{h_{j+1/2}}-1\Big)\Big]|u'_{j+1}(t)-u'_j(t)|^2\,dt \\ &+ \frac{1}{24}\sum_{j=0}^{N}\int_0^T \Big[\theta_{j+1}\Big(\frac{3h_{j+3/2}}{h_{j+1/2}}-1\Big) + \theta_j\Big(\frac{3h_{j-1/2}}{h_{j+1/2}}-1\Big)\Big]\big(|u'_{j+1}(t)|^2 - |u'_j(t)|^2\big)\,dt \\ =& \frac{1}{24}\sum_{j=0}^{N}\int_0^T \Big[\theta_{j+1}\Big(\frac{3h_{j+3/2}}{h_{j+1/2}}-1\Big) - \theta_j\Big(\frac{3h_{j-1/2}}{h_{j+1/2}}-1\Big)\Big]|u'_{j+1}(t)-u'_j(t)|^2\,dt \\ &- \frac{1}{24}\sum_{j=1}^{N}\int_0^T \Big[\theta_{j+1}\Big(\frac{3h_{j+3/2}}{h_{j+1/2}}-1\Big) + 3\theta_j\Big(\frac{h_{j-1/2}}{h_{j+1/2}} - \frac{h_{j+1/2}}{h_{j-1/2}}\Big) - \theta_{j-1}\Big(\frac{3h_{j-3/2}}{h_{j-1/2}}-1\Big)\Big]|u'_j(t)|^2\,dt.\end{aligned}$$

Combining all the above computations yields the identity (5.6). □

We then derive the counterpart of Proposition 2.2:

Proposition 5.4. *Let $g : [0,1] \to [0,1]$ be a C^3-diffeomorphism with $g(0) = 0$, $g(1) = 1$. Let $N \in \mathbb{N}$, $h = 1/(N+1)$. To simplify notations, we extend g as a C^3 function in a neighborhood of $[0,1]$ and for h small enough, we set $h_{-1/2}$, h_0, $h_{N+3/2}$, h_{N+1} as in (2.4). We choose $\theta_0 > 0$ and for $j \in \{0, \cdots, N+1\}$, we set θ_j as in (2.5).*

Using the same notations as in Proposition 2.2 and (2.10), we get the straightforward identities:

$$\theta_{N+1} = 1 + \theta_0, \qquad \theta_j \geq 0, \quad \theta_{j+1} - \theta_j = h_{j+1/2}, \qquad \forall j \in \{0, \cdots, N+1\},$$

and the following Taylor expansions:

$$\frac{h_{j-1/2}}{h_{j+1/2}} - \frac{h_{j+1/2}}{h_{j-1/2}} = -\frac{2g_j''}{g_j'} h + \mathcal{O}(h^2), \tag{5.7}$$

$$\begin{aligned} \theta_{j+1}\Big(\frac{h_{j+1/2}}{h_{j+3/2}} + \frac{2h_{j+3/2}}{h_{j+1/2}} - 1\Big) + \theta_j\Big(1 - \frac{2h_{j-1/2}}{h_{j+1/2}} - \frac{h_{j+1/2}}{h_{j-1/2}}\Big) \\ = \frac{2h}{g'_{j+1/2}}\Big((\theta_0 + g_{j+1/2})g''_{j+1/2} + (g'_{j+1/2})^2\Big) + \mathcal{O}(h^2), \end{aligned} \tag{5.8}$$

$$\theta_{j+1}\Big(\frac{3h_{j+3/2}}{h_{j+1/2}} - 1\Big) + 3\theta_j\Big(\frac{h_{j-1/2}}{h_{j+1/2}} - \frac{h_{j+1/2}}{h_{j-1/2}}\Big) - \theta_{j-1}\Big(\frac{3h_{j-3/2}}{h_{j-1/2}} - 1\Big) = 4h_j + \mathcal{O}(h^2). \tag{5.9}$$

Proof. The proof of (5.7)–(5.8)–(5.9) is based on the Taylor expansions in (2.9), (2.11) and explicit computations. The detailed computations are very similar to the ones in Proposition 2.2 and are therefore left to the reader. □

We are now in position to prove Theorem 5.1.

Proof of Theorem 5.1. Let g be a smooth strictly concave function, in which case (5.7) can be reinforced in

$$\frac{h_{j-1/2}}{h_{j+1/2}} - \frac{h_{j+1/2}}{h_{j-1/2}} \geq 0.$$

We then take the multiplier (2.1) with θ as in (2.5). Using Proposition 5.3 and Proposition 5.4, we derive:

$$\begin{aligned} &\sum_{j=1}^{N}\Big(\frac{h_{j+1/2}}{6}u'_{j+1}(t) + \frac{2h_j}{3}u'_j(t) + \frac{h_{j-1/2}}{6}u'_{j-1}(t)\Big)m_j(t)\Big|_0^T \\ &+ \frac{1}{6}\sum_{j=1}^{N}\int_0^T \Big(h_j + \mathcal{O}(h^2)\Big)|u'_j(t)|^2\,dt \\ &+ \frac{1}{12}\sum_{j=0}^{N}\int_0^T h_{j+1/2}|u'_{j+1}(t) + u'_j(t)|^2\,dt + \frac{1}{2}\sum_{j=0}^{N}\int_0^T h_{j+1/2}\left|\frac{u_{j+1}(t) - u_j(t)}{h_{j+1/2}}\right|^2 dt \\ &- \frac{1}{12}\sum_{j=0}^{N}\int_0^T \Big(\frac{h}{g'_{j+1/2}}\Big((\theta_0 + g_{j+1/2})g''_{j+1/2} + (g'_{j+1/2})^2\Big) + \mathcal{O}(h^2)\Big)|u'_{j+1}(t) - u'_j(t)|^2\,dt \\ &\leq \left(\frac{1+\theta_0}{12}\right)\int_0^T |u'_N(t)|^2\,dt + \left(\frac{(1+\theta_0}{2}\right)\int_0^T \left|\frac{u_N(t)}{h_{N+1/2}}\right|^2 dt. \end{aligned} \tag{5.10}$$

Taking into account the conservation in time of the total energy, we get

$$\frac{1}{6}\sum_{j=1}^{N}\int_0^T h_j|u_j'(t)|^2\,dt+\frac{1}{12}\sum_{j=0}^{N}\int_0^T h_{j+1/2}|u_{j+1}'(t)+u_j'(t)|^2\,dt \\ +\frac{1}{2}\sum_{j=0}^{N}\int_0^T h_{j+1/2}\left|\frac{u_{j+1}(t)-u_j(t)}{h_{j+1/2}}\right|^2\,dt=TE_f^{h,g}(\mathbf{u}^{0,h},\mathbf{u}^{1,h}). \quad (5.11)$$

Besides, choosing $\theta_0=\theta_g$ as in (1.9), we have $(\theta_0+g_{j+1/2})g''_{j+1/2}+(g'_{j+1/2})^2\le 0$, so that

$$-\frac{1}{12}\sum_{j=0}^{N}\int_0^T\Big(\frac{h}{g'_{j+1/2}}\Big((\theta_0+g_{j+1/2})g''_{j+1/2}+(g'_{j+1/2})^2\Big)+\mathcal{O}(h^2)\Big)|u'_{j+1}(t)-u'_j(t)|^2\,dt \\ +\frac{1}{6}\sum_{j=1}^{N}\int_0^T\mathcal{O}(h^2)|u_j'(t)|^2\,dt\ge -CThE_f^{h,g}(\mathbf{u}^{0,h},\mathbf{u}^{1,h}).$$

In order to conclude, we then simply have to estimate the time boundary terms in (5.10). By Cauchy Schwartz inequality, we have

$$\left|\sum_{j=1}^{N}\Big(\frac{h_{j+1/2}}{6}u'_{j+1}(t)+\frac{2h_j}{3}u'_j(t)+\frac{h_{j-1/2}}{6}u'_{j-1}(t)\Big)m_j(t)\right| \\ \le\frac{1+\theta_g}{2}\left(\sum_{j=1}^{N}\frac{1}{h_j}\Big(\frac{h_{j+1/2}}{6}u'_{j+1}(t)+\frac{2h_j}{3}u'_j(t)+\frac{h_{j-1/2}}{6}u'_{j-1}(t)\Big)^2\right)^{1/2}\left(\sum_{j=1}^{N}h_j\Big|\frac{2m_j}{\theta_j}\Big|^2\right)^{1/2}.$$

The first term can be bounded as follows:

$$\begin{aligned}
&\sum_{j=1}^{N}\frac{1}{h_j}\Big(\frac{h_{j+1/2}}{6}u'_{j+1}(t)+\frac{2h_j}{3}u'_j(t)+\frac{h_{j-1/2}}{6}u'_{j-1}(t)\Big)^2\\
&=\sum_{j=1}^{N}\frac{1}{h_j}\Big(\frac{h_{j+1/2}}{6}(u'_{j+1}+u'_j)+\frac{h_j}{3}u'_j+\frac{h_{j-1/2}}{6}(u'_j+u'_{j-1})\Big)^2\\
&\le\frac{3}{2}\sum_{j=1}^{N}\frac{1}{h_j}\Big(\frac{h_{j+1/2}}{6}(u'_{j+1}+u'_j)+\frac{h_{j-1/2}}{6}(u'_j+u'_{j-1})\Big)^2+3\sum_{j=1}^{N}\frac{h_j}{9}|u'_j|^2\\
&\le 3\sum_{j=1}^{N}\frac{1}{h_j}\Big(\frac{h_{j+1/2}}{6}(u'_{j+1}+u'_j)\Big)^2+3\sum_{j=1}^{N}\frac{1}{h_j}\Big(\frac{h_{j-1/2}}{6}(u'_j+u'_{j-1})\Big)^2+\frac{1}{3}\sum_{j=1}^{N}h_j|u'_j|^2\\
&\le\frac{1}{6}\sum_{j=0}^{N}h_{j+1/2}(u'_{j+1}+u'_j)^2+\frac{1}{3}\sum_{j=1}^{N}h_j|u'_j|^2+Ch^2E_f^{h,g}(\mathbf{u}^{0,h},\mathbf{u}^{1,h}).
\end{aligned}$$

Recalling (2.15), we then easily get

$$\left|\sum_{j=1}^{N}\Big(\frac{h_{j+1/2}}{6}u'_{j+1}(t)+\frac{2h_j}{3}u'_j(t)+\frac{h_{j-1/2}}{6}u'_{j-1}(t)\Big)m_j(t)\right|\le(1+\theta_g)(1+Ch^2)E_f^{h,g}(\mathbf{u}^{0,h},\mathbf{u}^{1,h}).$$

Putting together all the above estimates in (5.10), we obtain

$$(T(1-Ch)-2(1+\theta_g)(1+Ch^2))E_f^{h,g}(\mathbf{u}^{0,h},\mathbf{u}^{1,h}) \\ \leq \left(\frac{1+\theta_0}{12}\right)\int_0^T |u_N'(t)|^2\,dt + \left(\frac{1+\theta_0}{2}\right)\int_0^T \left|\frac{u_N(t)}{h_{N+1/2}}\right|^2 dt. \quad (5.12)$$

This concludes the proof of Theorem 5.1. □

6 Further comments and open problems

In this section we discuss some issues, closely related to the topics addressed in this paper and that would be worth to investigate in the future.

Unstructured meshes. Our analysis suggests that a suitable way to re-establish uniform observability for space semi-discrete wave equations is to work with meshes which are refined close to the observation set. So far, we performed our analysis on meshes which can be obtained as the image of a diffeormorphism from $[0,1]$ to itself to be able to perform Taylor expansions in Proposition 2.2. But one can easily check from the proof in Section 2 that uniform observability properties can be recovered for sequences of meshes $\mathscr{M}^h$, not necessarily obtained as the diffeomorphic image of the uniform mesh, given by N ($h=1/(N+1)$) points $\{0<x_1^h<\cdots<x_N^h<1\}$ characterized by two constants M and r independent of h as follows:

- an almost uniform mesh size: for all $h>0$,

$$\frac{\sup_j h_{j+1/2}}{\inf_j h_{j+1/2}} \leq r, \quad (6.1)$$

- the existence of a discrete function $\theta=(\theta_j^h)_{j\in\{0,\cdots,N+1\}}$ for which

$$\begin{cases} \dfrac{\theta_j h_j+\theta_{j+1}h_{j+1}}{h_{j+1/2}} - \dfrac{\theta_{j-1}h_{j-1}+\theta_j h_j}{h_{j-1/2}} \geq 2h_j - o(h), & j\in\{1,\cdots,N\}. \\ \theta_{j+1}h_{j+1}-\theta_j h_j \leq o(h^3), & j\in\{0,\cdots,N\}, \\ \theta_{j+1}\ -\theta_j \geq h_{j+1/2}-o(h), & j\in\{0,\cdots,N\}, \\ \theta_0\geq 0, \quad \theta_{N+1}\leq M. \end{cases} \quad (6.2)$$

In that case, the corresponding equations (1.5) are uniformly observable in any time $T>2M$.

Note that in the above condition (6.2), we assume, for all $j\in\{0,\cdots,N\}$, that

$$\theta_{j+1}\geq\theta_j+h_{j+1/2}-o(h), \quad \text{and} \quad \theta_{j+1}\leq\theta_j\frac{h_j}{h_{j+1}}+o(h^2), \quad j\in\{0,\cdots,N\},$$

so that necessarily such meshes satisfy $h_j/h_{j+1}\geq 1$. This implies that sequence of meshes satisfying (6.1)–(6.2) necessarily are refined close to the observation set $x=1$.
Note however that a complete characterization of all the sequences of meshes satisfying (6.1)–(6.2) seems difficult to establish.

Time discrete and fully discrete approximation schemes of (1.1)**.** In this article, we focused on the space semi-discrete approximation of (1.1). In order to extend our analysis to the case of fully discrete approximation schemes of (1.1), we can apply the results in [8] decoupling the effects of the time and space semi-discretizations. In our context for instance, this would imply that if we consider

a fully discrete approximation of (1.1) obtained from (1.5) for a concave function $g : [0,1] \to [0,1]$ and discretized in time using the midpoint approximation scheme with time step Δt, the fully discrete systems obtained that way are uniformly observable in any time T satisfying

$$T > T_g \left(1 + \frac{\delta^2}{4}\right), \text{ with } \delta \geq (\Delta t)\, \sqrt{\lambda^{N,h,g}},$$

where $\lambda^{N,h,g}$ is the largest eigenvalue of the elliptic problem (3.2) corresponding to the mesh $\mathscr{M}^{h,g}$. Easy estimates show that $\lambda^{N,h,g} \leq 4/\inf_j h_{j+1/2}^2 \leq 4/(hg'(1))^2$. Thus, the condition $\delta \geq (\Delta t)\, \sqrt{\lambda^{N,h,g}}$ can be replaced by the more usual Courant-Friedrichs-Levy (CFL) type condition

$$\frac{2\Delta t}{h} \leq \delta g'(1).$$

We refer to [8, Section 5.2] for more extensive details.

Rates of convergence of the discrete controls. Following the proofs in [10] or [11] one could also analyse the rate of convergence of the numerical schemes developed in this article, and, in particular, obtain the rate of convergence of the controls. But, even if major new difficulties are not expected with respect to the work previously developed in the context of uniform meshes, this requires further investigation.

Higher dimensional settings. So far, our results are restricted to the $1d$ case. However, it is very likely that our approach can be generalized to higher dimensional setting under the condition that the mesh has to be finer close to the observation set. But this requires further work. In particular, we should recall that, in $2d$, even the classical property of unique continuation of eigenfunctions may fail at the discrete level (see the counterexample of O. Kavian described in [28]).

Inverse problems. Observability estimates can also be used directly to recover the initial datum of solutions of (1.5) from a measurement of the flux on the boundary $x = 1$, thus indicating a first possible use of the results in this paper in the context of Inverse problems.

To be more precise, assume that the flux $\partial_x u(t,1)$ for some unknown solution of the wave equation (1.1) is known, by means of some measurement device, and let us build a numerical algorithm allowing to obtain numerical approximations of the corresponding initial datum (u^0, u^1) in (1.1). We proceed by minimizing the functional

$$J^h(\mathbf{u}^{0,h}, \mathbf{u}^{1,h}) = \frac{1}{2} \int_0^T \eta(t) \left| \frac{u_N^h(t)}{h_{N+1/2}} + \partial_x u(t,1) \right|^2 dt,$$

for all solutions $\mathbf{u}^h$ of (1.5), which shares the same features of the functional in (4.7) introduced to compute the discrete controls corresponding to some initial data.

When uniform observability properties hold for (1.5) in time T and the observation is done during a period T, the discrete minimizers $(\mathbf{U}^{0,h}, \mathbf{U}^{1,h})$ (or, to be more precise, their continuous extension) converge to (u^0, u^1) in $H_0^1(0,1) \times L^2(0,1)$ as $h \to 0$ (see [11, Section 1.8]). This fact provides a first example of the use of these non-uniform grids in the context of inverse problems. We also refer to the works [15] for another strategy (based on the used of back and forth observers) in a situation in which the observability property does not necessarily hold uniformly with respect to the discretization parameters.

This idea of using suitable non-uniform grids could also be helpful for proving convergence results for other inverse problems, similar to the ones developed in [3, 4] in the context of uniform grids. In these works, the convergence of discrete inverse problems is proved by adding some penalization on the high-frequency components of the solutions, which was needed to avoid to deal with the spurious high-frequency waves created by uniform meshes. It would be interesting to investigate whether, using these non-uniform grid, these extra penalization terms could be avoided.

References

[1] C. Bardos, G. Lebeau, and J. Rauch. Un exemple d'utilisation des notions de propagation pour le contrôle et la stabilisation de problèmes hyperboliques. *Rend. Sem. Mat. Univ. Politec. Torino*, (Special Issue):11–31 (1989), 1988. Nonlinear hyperbolic equations in applied sciences.

[2] C. Bardos, G. Lebeau, and J. Rauch. Sharp sufficient conditions for the observation, control and stabilization of waves from the boundary. *SIAM J. Control and Optim.*, 30(5):1024–1065, 1992.

[3] L. Baudouin and S. Ervedoza. Convergence of an inverse problem for a 1-D discrete wave equation. *SIAM J. Control Optim.*, 51(1):556–598, 2013.

[4] L. Baudouin, S. Ervedoza, and A. Osses. Stability of an inverse problem for the discrete wave equation and convergence results. *J. Math. Pures Appl., to appear.*

[5] L. Borcea and V. Druskin. Optimal finite difference grids for direct and inverse Sturm-Liouville problems. *Inverse Problems*, 18(4):979–1001, 2002.

[6] L. Borcea, V. Druskin, and L. Knizhnerman. On the continuum limit of a discrete inverse spectral problem on optimal finite difference grids. *Comm. Pure Appl. Math.*, 58(9):1231–1279, 2005.

[7] S. Ervedoza. Observability properties of a semi-discrete 1D wave equation derived from a mixed finite element method on nonuniform meshes. *ESAIM Control Optim. Calc. Var.*, 16(2):298–326, 2010.

[8] S. Ervedoza and E. Zuazua. Transmutation techniques and observability for time-discrete approximation schemes of conservative systems. *Numer. Math., to appear*, doi 10.1007/s00211-014-0668-3.

[9] S. Ervedoza and E. Zuazua. A systematic method for building smooth controls for smooth data. *Discrete Contin. Dyn. Syst. Ser. B*, 14(4):1375–1401, 2010.

[10] S. Ervedoza and E. Zuazua. The wave equation: Control and numerics. In P. M. Cannarsa and J. M. Coron, editors, *Control of Partial Differential Equations*, Lecture Notes in Mathematics, CIME Subseries. Springer Verlag, 2011.

[11] S. Ervedoza and E. Zuazua. *Numerical approximation of exact controls for waves.* Springer Briefs in Mathematics. Springer, New York, 2013.

[12] R. Glowinski. Ensuring well-posedness by analogy: Stokes problem and boundary control for the wave equation. *J. Comput. Phys.*, 103(2):189–221, 1992.

[13] R. Glowinski and C. H. Li. On the numerical implementation of the Hilbert uniqueness method for the exact boundary controllability of the wave equation. *C. R. Acad. Sci. Paris Sér. I Math.*, 311(2):135–142, 1990.

[14] R. Glowinski, C. H. Li, and J.-L. Lions. A numerical approach to the exact boundary controllability of the wave equation. I. Dirichlet controls: description of the numerical methods. *Japan J. Appl. Math.*, 7(1):1–76, 1990.

[15] G. Haine and K. Ramdani. Reconstructing initial data using observers: error analysis of the semi-discrete and fully discrete approximations. *Numer. Math.*, 120(2):307–343, 2012.

[16] J.A. Infante and E. Zuazua. Boundary observability for the space semi discretizations of the 1-d wave equation. *Math. Model. Num. Ann.*, 33:407–438, 1999.

[17] A. E. Ingham. Some trigonometrical inequalities with applications to the theory of series. *Math. Z.*, 41(1):367–379, 1936.

[18] J.-L. Lions. *Contrôlabilité exacte, Stabilisation et Perturbations de Systèmes Distribués. Tome 1. Contrôlabilité exacte*, volume RMA 8. Masson, 1988.

[19] F. Macià. *Propagación y control de vibraciones en medios discretos y continuos.* PhD thesis, Universidad Complutense de Madrid, 2001.

[20] A. Marica and E. Zuazua. Propagation of 1-D waves in regular discrete heterogeneous media: a Wigner measure approach. *J. FoCM* , 2014, doi 10.1007/s10208-014-9232-x.

[21] S. Micu and E. Zuazua. Boundary controllability of a linear hybrid system arising in the control of noise. *SIAM J. Cont. Optim.*, 35(5):1614-1638, 1997.

[22] S. Micu. Uniform boundary controllability of a semi-discrete 1-D wave equation. *Numer. Math.*, 91(4):723–768, 2002.

[23] L. Miller. Resolvent conditions for the control of unitary groups and their approximations. *J. Spectr. Theory*, 2(1):1–55, 2012.

[24] M. Negreanu and E. Zuazua. Convergence of a multigrid method for the controllability of a 1-d wave equation. *C. R. Math. Acad. Sci. Paris*, 338(5):413–418, 2004.

[25] J. V. Ralston. Solutions of the wave equation with localized energy. *Comm. Pure Appl. Math.*, 22:807–823, 1969.

[26] L. N. Trefethen. Group velocity in finite difference schemes. *SIAM Rev.*, 24(2):113–136, 1982.

[27] R. Vichnevetsky. Wave propagation and reflection in irregular grids for hyperbolic equations. *Appl. Numer. Math.*, 3(1-2):133–166, 1987.

[28] E. Zuazua. Propagation, observation, and control of waves approximated by finite difference methods. *SIAM Rev.*, 47(2):197–243 (electronic), 2005.